Submission to ***ACS Applied Materials & Interfaces***

Multilayered Shape-morphing Scaffolds with a Hierarchical Structure for Uterine Tissue Regeneration

Shangsi Chen [a, 1], Shenglong Tan [b, 1], Liwu Zheng [c], Min Wang [a, *]

[a] Department of Mechanical Engineering

The University of Hong Kong

Pokfulam Road, Hong Kong

[b] Department of Endodontics and Operative Dentistry

College of Stomatology, Southern Medical University

No. 1838 North Guangzhou Avenue, Guangzhou, China

[c] Faculty of Dentistry

The University of Hong Kong

34 Hospital Road, Sai Ying Pun, Hong Kong

Keywords: uterine tissue engineering, multilayer film, 3D bioprinting, cell-laden hydrogel, controlled release, shape morphing

---

[1] These authors contributed equally to this work.

* Corresponding Author:

Professor Min Wang, at the University of Hong Kong, Hong Kong

Email: memwang@hku.hk Tel: +852 3917 7903 Fax: +852 28585415

Abstract

Owing to dysfunction of the uterus, millions of couples around the world suffer from infertility. Different from conventional treatments, tissue engineering provides a new and promising approach to deal with difficult problems of human tissue or organ failure. Adopting scaffold-based tissue engineering, three-dimensional (3D) porous scaffolds in combination with stem cells and appropriate biomolecules may be constructed for uterine tissue regeneration. In this study, a hierarchical tissue engineering scaffold, which mimicked the uterine tissue structure and functions, was designed and the biomimicking scaffolds were then successfully fabricated using solvent casting, layer-by-layer assembly and 3D bioprinting techniques. For the multilayered, hierarchical structured scaffolds, poly(L-lactide-co-trimethylene carbonate) (PLLA-co-TMC, "PLATMC" in short) and poly(lactic acid-co-glycolic acid) (PLGA) blends were firstly used to fabricate the shape-morphing layer of the scaffolds, which was to mimic the function of myometrium in uterine tissue. The PLATMC/PLGA polymer blend scaffolds were highly stretchable. Subsequently, after etching of the PLATMC/PLGA surface and employing estradiol (E2), polydopamine (PDA) and hyaluronic acid (HA), PDA@E2/HA multilayer films were formed on PLATMC/PLGA scaffolds to build an intelligent delivery platform to enable controlled and sustained release of E2. The PDA@E2/HA multilayer films also improved the biological performance of the scaffold. Finally, a layer of bone marrow-derived mesenchymal stem cell (BMSC)-laden hydrogel (which was a blend of gelatin methacryloyl (GelMA) and gelatin (Gel)) was 3D printed on the PDA@E2/HA multilayer films of the scaffold, thereby completing the construction of the hierarchical scaffold. BMSCs in the GelMA/Gel hydrogel layer exhibited excellent cell viability and could spread and be released eventually upon the biodegradation of the GelMA/Gel hydrogel. It was shown that the hierarchical structured scaffolds could evolve from the initial flat shape into the tubular structure completely in an aqueous environment at 37°C, fulfilling the requirement for curved scaffolds for uterine tissue engineering. The biomimicking scaffolds with a hierarchical structure and curved shape, high stretchability, and controlled and sustained E2 release appear very promising for uterine tissue regeneration.

1. Introduction

Reproduction is one the most important functions of human beings. Giving birth to healthy babies is essential for the development of a modern society. Unfortunately, numerous couples at the child-bearing age suffer from infertility. According to the definition by the World Health Organization (WHO), infertility is the inability to achieve a clinical pregnancy after 1-year regular unprotected sexual intercourses between male and female couples [1]. A recent report pointed out that because of infertility, more than 14% of females at reproductive ages (from 12 to 49 years old) could not conceive or carry a viable fetus to term as they had desired. About 0.2% of women are diagnosed for absolute uterine factor infertility (AUFI) owing to the damage or dysfunction of the uterus [2]. Allogeneic uterus transplantation is a practical option to deal with uterine injuries and hence can help to realize the dreams of many couples to become biological parents of their children [3]. Dozens of publications have already reported successful live births by women who had received transplanted uteri [4, 5]. However, facing problems of donor shortage and possible immunological rejection, uterus transplantation cannot be widely practiced. Therefore, new and promising clinical treatments should be developed to treat uterine damages, which will assist reconstructing the structure and restoring the functions of human uterus.

The tissue engineering approach emerged three decades ago and has been applied for regenerating various human body tissues to overcome the problems of donor organ shortage and limitations of allogeneic transplantation. In scaffold-based tissue engineering, a crucial task is the fabrication of a three-dimensional (3D) structure to mimic the anatomical structure and provide essential functions of the targeted tissue through the combination of suitable biomaterials (synthetic or natural) and cells (mature cells or stem cells, particularly autologous stem cells in recent years) and with the incorporation of appropriate biomolecules (which guide cell behavior and new tissue formation). Therefore, using tissue engineering strategies to create biological substitutes based on the combination of autologous cells with biomaterials and biomolecules provides a promising approach for uterine regeneration [6]. In fact, tissue engineering strategies are gradually applied to uterus, with uterine scaffolds being constructed to treat uterine injuries [7, 8]. For example, Li *et al.* produced a collagen membrane loaded with

human basic fibroblast growth factor (bFGF) for repairing uterine damage [9]. They found that the implanted collagen membrane could sustainably deliver bFGF, thus improving regeneration abilities of uterine endometrium and muscular cells and promoting angiogenesis and pregnancy rate. In another study, bone marrow-derived mesenchymal stem cell (BMSC)-incorporated poly(glycerol sebacate) (PGS) tissue engineering scaffolds were constructed for restoring the morphology and functions of wounded uterus [10]. It was shown that BMSC/PGS scaffolds could facilitate endometrium regeneration, resulting in better uterus morphology recovery and fertility improvement.

Although the combination of biomaterials, cells and biomolecules to form uterine tissue engineering scaffolds holds great promise in enhancing the regeneration ability in uterine reconstruction, currently, most studies have focused only on endometrium regeneration while restoring myometrium functions has not been sufficiently addressed. Myometrium regeneration is also crucial for the reconstruction of uterine tissue structure and functions. However, studies so far have mainly focused on endometrium regeneration, with research rarely being conducted for myometrium regeneration. The human uterine tissue has a hierarchical structure, with myometrium and endometrium being the two main parts of the uterine tissue (Fig.1A). Myometrium comprises smooth muscle cells and its primary functions are to induce contraction and expansion and support stromal and vascular tissues. The uterine contraction is contraction of the smooth muscle in the uterus that occurs during both the menstrual cycle and labor, indicating the importance of myometrium for embryonic development. Endometrium is a unique and dynamic tissue that undergoes cyclic growth and tissue remodeling and is essential for embryo implantation and development. In clinical treatments, the whole uterus regeneration involving both endometrium and myometrium should be considered. Recently, Magalhaes *et al.* fabricated a uterine tissue engineering scaffold using biodegradable polymers seeded with autologous cells and used rabbits to assess the construction of uterine structure and restoration of uterus functions [11]. Their scaffolds could lead to the formation of uterus-like structures, including endometrium (stroma, glandular epithelium) and myometrium, which resulted in successful pregnancy and supported fetal development after 6-month implantation of the scaffold. However, their scaffolds did not

appear to be optimally designed, considering the hierarchical structure, biological complexity, and highly elastic nature of human uterus. Their simple poly(lactic acid-co-glycolic acid) (PLGA)/poly(glycolic acid) (PGA) scaffolds without the desirable hierarchical architecture and high elasticity could not immediately restore the intrinsic functions of the uterus after their implantation in the body.

For fabricating tissue engineering scaffolds with hierarchical structures and biological complexity, 3D printing provides a powerful manufacturing platform. 3D printing was started in 1986 and has been applied rapidly in tissue engineering and regenerative medicine in recent years [12, 13]. Tissue engineering scaffolds produced by 3D printing have been widely used for regenerating a variety of human body tissues, including bone, articular cartilage, skin, blood vessel and nerve [14-17]. 3D printing technologies have now become popular methods for fabricating patient-specific scaffolds which are anatomically similar to native tissues with their complex and hierarchical structures [18]. The utilization of 3D printed advanced tissue engineering scaffolds should provide significant impetus for uterine regeneration. Indeed, several studies have been reported for using 3D printing technologies to construct uterine tissue engineering scaffolds [19, 20]. Li *et al.* reported the possibility of employing 3D bioprinted hydrogels to repair endometrium [21]. They prepared a bioink of alginate hydrogel encapsulated with human induced pluripotent stem cell-derived mesenchymal stem cells (hiMSCs) and then 3D printed cell-laden hydrogel scaffolds for treating endometrial damages. But apart from these few reports, applying 3D printing in uterine tissue engineering has been rarely reported. Furthermore, using shape morphing materials in 3D printing to fabricate curved structures for uterine regeneration has not been seen so far.

In the current study, tissue engineering scaffolds were fabricated via 3D printing which would mimic human uterus's hierarchical architecture and assume its curved shape (see Fig.1B and C for the schematic illustration of scaffold fabrication). Briefly, polymer blend scaffolds with high elasticity were firstly made using poly(L-lactide-co-trimethylene carbonate) (PLLA-co-TMC, "PLATMC" in short) and PLGA as a base layer for mimicking myometrium. Subsequently, hyaluronic acid (HA) and polydopamine (PDA) particles encapsulated with estradiol (E2) (PDA@E2) were alternatively coated on the PLATMC/PLGA scaffold via layer-

by-layer self-assembly. E2 is a steroid hormone that has been clinically used for promoting uterine regeneration by binding to its receptors and then activating the expression of various angiogenic growth factors. In previous studies, PDA particles were extensively used as a drug carrier for controlled release because of their excellent biocompatibility, pH-sensitive property and photo-thermal effect [22]. In the current study, PDA particles were employed as an E2 controlled release vehicle, protecting the bioactivity and maintaining the effectiveness of E2. The PDA@E2/HA multilayer films would act as an intelligent E2 delivery platform and improve the biological performance. Finally, a layer of BMSC-laden gelatin methacryloyl (GelMA)/gelatin (Gel) hydrogel which mimicked the structure and functions of endometrium was 3D printed on the deposited PDA@E2/HA multilayer films. This complex and hierarchical construct was designed to possess high stretchability and controllable E2 delivery. Furthermore, the scaffold would change from its planar shape at room temperature to the curved structure via programmed shape morphing when it is put in an aqueous environment at the human body temperature of 37℃. This scaffold with a biomimicking hierarchical structure is expected to have high potential in uterine tissue engineering. Compared to previous investigations into uterine tissue regeneration which mainly focused on endometrium regeneration, the current study has investigated novel trilayer scaffolds for regenerating both endometrium and myometrium for functional regeneration of the uterine tissue.

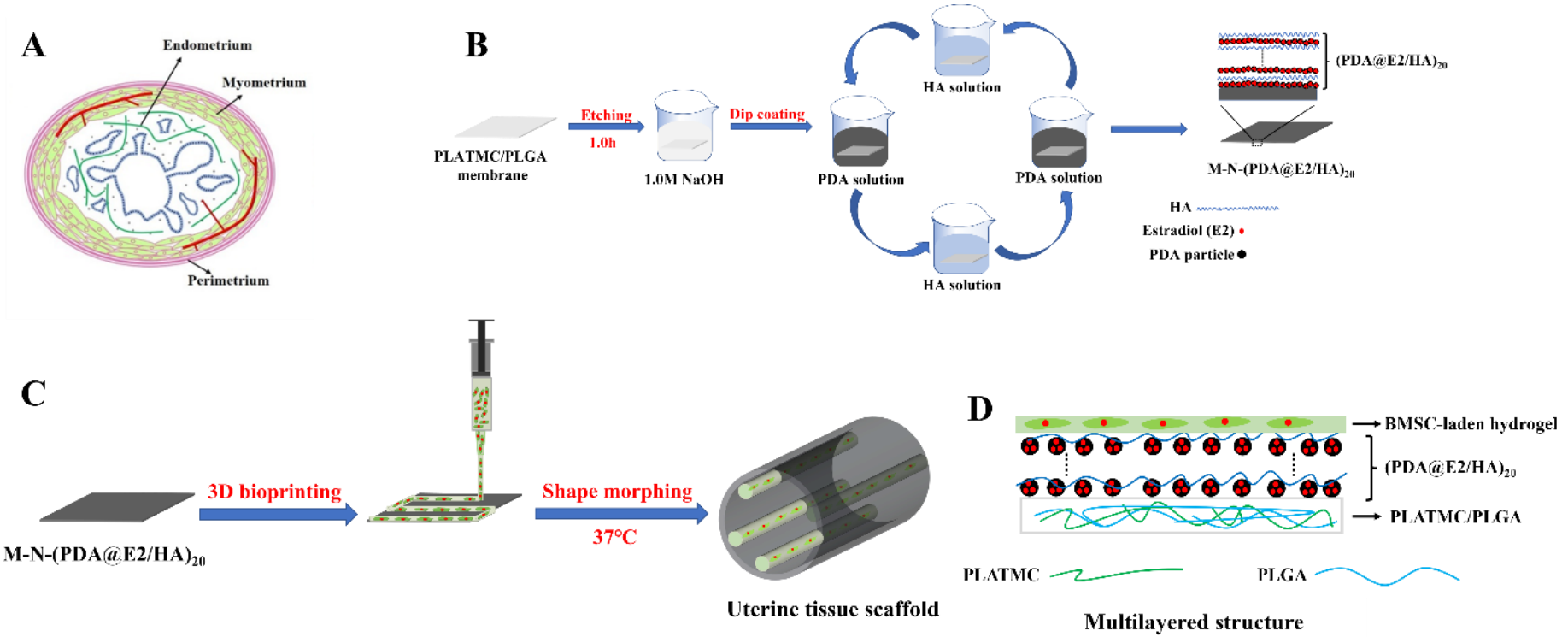

Fig.1 Schematic illustration for the uterine tissue and fabrication of biomimicking uterine tissue engineering scaffolds. (A) Schematic illustration (cross-sectional view) of the hierarchical structure of the uterine tissue. (B) Fabrication of PDA@E2/HA multilayer films on the surface of PLATMC/PLGA scaffold. (C) Fabrication of 3D printed BMSC-laden GelMA/Gel layer on the $(PDA@E2/HA)_{20}$ multilayer films of PLATMC/PLGA scaffold and shape morphing behavior of the final uterine tissue engineering scaffold. (D) Schematic illustration showing the layered structure of multilayered uterine tissue scaffolds.

2. Materials and Methods

2.1 Materials

Poly(L-lactide-co-trimethylene carbonate) (PLLA-co-TMC: "PLATMC" in short, with a molar ratio of LA: TMC = 8: 2 and dl/g 0.9, as well as those with LA: TMC molar ratio of 9:1 and 5:5) and poly(lactic acid-co-glycolic acid) (PLGA, with a molar ratio of LA: GA =50: 50 and average molecular weight of 90KDa) were purchased from Jinan Daigang Ltd., China. Gelatin (porcine skin, type A), methacrylate anhydride (MA, 94%), ammonium hydroxide solution (NH_4OH) (28%), sodium hydroxide (NaOH), absolute ethanol, 2-hydroxy-2-methylpropiophenone (97%, photoinitiator) were bought from Sigma-Aldrich (St. Louis, MO, USA). Dopamine hydrochloride (DA, 98%), β-estradiol (E2, 99%), hyaluronic acid sodium salt from streptococcus equl (95%) were supplied by Aladdin Co. Ltd., China. Dichloromethane (DCM) was bought from RCI Labscan Ltd., Thailand. Dialysis tubing cellulose membrane (MWCO 10kDa) was supplied by Thermo Fisher Scientific, USA. All reagents were used as-received without further purification.

2.2 Fabrication of PLATMC/PLGA scaffolds and surface modification

4.0g PLATMC and 1.0g PLGA were dissolved in 20ml DCM under constant magnetic stirring. The obtained polymer solution was poured into a 10-inch glass peri dish and placed in a fume hood at room temperature for at least one week for the complete evaporation of the organic solvent DCM. Subsequently, the flat PLATMC/PLGA scaffolds after casting (designated as M scaffolds) were shaped into the tubular structure using a stainless- teel rod (rod diameter: 8mm) in an oven at 50℃ for 30min. Afterwards, the tubular scaffolds were flattened at room temperature for further use.

Because the poor hydrophilicity and very flat surface of M scaffolds were not beneficial for the fabrication of multilayer films on their surface, NaOH solution was therefore used to generate carboxylate and hydroxyl groups and to increase the surface roughness of M scaffolds through the hydrolysis process. In brief, M scaffolds were immersed in NaOH solutions of different concentrations (0.1, 0.5, 1.0, 2.0, and 5.0M) for different times (0.5, 1.0, 2.0, 4.0, 8.0, 12.0,

24.0, and 48.0h) at room temperature (3 samples for each experiment). Afterwards, the wettability of thus treated scaffolds (designated as M-N scaffolds) was assessed using water contact angle measurement. M-N scaffolds were coated with a thin layer of gold by sputtering and then observed under a scanning electron microscope (SEM, Hitachi S-4800, Japan).

2.3 Synthesis of PDA@E2 particles

The synthesis of PDA and PDA@E2 particles was similar to the previously reported procedures [23, 24] but with some modifications. Estradiol (E2) is poorly water-soluble. To increase its solubility, an ethanol/water mixture was used for synthesizing PDA@E2 particles. Different amounts of E2 (0, 0.25, 0.5, and 0.75g) were dissolved separately in 350ml ethanol under constant magnetic stirring for at least 2h. 10ml ammonia and 290ml DI water were then added in the solutions under stirring for 30min. Subsequently, 2.5g dopamine hydrochloride was dissolved in 50ml DI water. The dopamine solution was then poured into the ethanol/water mixture under constant stirring for 24h at room temperature in open air. Finally, PDA and PDA@E2 particles were obtained by centrifuging at 12,000rpm/min for 10min and freeze-dried before storage. PDA particles were synthesized without E2 addition. Based on the amount of E2 used, the synthesized particles were designated as PDA (0g), PDA-0.1 (0.25g), PDA-0.2 (0.5g), and PDA-0.3 (0.75g), respectively.

The E2 loading efficiency in PDA particles was calculated according to the following formula:

$$\text{Loading efficiency (\%)} = [(M_1 - M_2)/M_1] \times 100\% \quad (1)$$

where M_1 and M_2 were the total mass of E2 added in the ethanol/water mixture and the remaining mass of E2 in the final solution, respectively. The morphology and structure of PDA and PDA@E2 particles were characterized using SEM and a transmission electron microscope (TEM, Tecnai G2 20, USA). The diameter distribution of PDA or PDA@E2 particles was analyzed using Image J software.

2.4 Fabrication of PDA@E2/HA multilayer films on M-N scaffolds

The fabrication of PDA@E2/HA multilayer films on the M-N scaffold surface was to improve

interface biological response as well as constructing a smart E2 delivery vehicle for the sustained release of E2 to regulate cell behavior and improve angiogenesis and hormone cycle, thereby facilitating uterine regeneration after scaffold implantation. M-N scaffolds etched by 1M NaOH for 1h were used. Briefly, M-N scaffolds were immersed in PDA@E2 suspensions (2 mg/ml of PDA@E2 particles in 10mM Tris, pH 8.5) for 15min. Subsequently, M-N scaffolds coated with PDA@E2 particles were taken out and washed with DI water three times to remove free PDA@E2 particles. The scaffolds were then immersed in 1mg/ml HA solution for another 15min and washed with DI water three times to remove free HA polymer. The $(PDA@E2/HA)_n$ multilayer film was made on the surface of a M-N scaffold by repeating the above process multiple times (i.e., n times), where n represents the process cycles repeated and hence the number of PDA@E2/HA bilayer. The final products, M-N-$(PDA@E2/HA)_n$ scaffolds, were freeze-dried and stored in a desiccator for further studies.

2.5 Mechanical properties

The mechanical properties of scaffolds produced in this study were investigated through tensile tests (5 samples for each type of scaffolds) at room temperature using a universal testing machine (Model 5848, Instron Ltd., USA) with a 100N load cell. The scaffolds were cut into the standard dumbbell shape. The speed of all tensile tests was set at 100% strain/min. The ultimate tensile strength and elongation at fracture were determined from stress-strain curves. The Young's modulus was calculated from the slope of the initial linear region of each stress-strain curve.

2.6 Photothermal effect and *in vitro* E2 release behavior

To investigate the photothermal effect of M-N-$(PDA@E2/HA)_{20}$ scaffolds, scaffold samples were irradiated by a near-infrared (NIR) laser (wavelength: 808nm) at different power densities ($0.5W/cm^2$ and $1.0W/cm^2$). The temperature change caused by NIR irradiation was revealed by thermal images which were recorded using an infrared camera (GUIDE® EasIR-9, AutoNavi, China).

To study the effect of NIR laser irradiation on E2 release, M-N-$(PDA@E2/HA)_{20}$ scaffolds (3

samples) were irradiated at different power densities (0, 0.5, and 1.0 W/cm^2) of the NIR laser for 30min every 1 hour in phosphate buffered saline (PBS, pH 7.4) at 37℃. The release medium was collected at each predetermined time point, and an equal amount of fresh PBS was added to the immersion liquid. The amount of E2 released in the immersion liquid was determined using a UV-vis spectrophotometer (UV-2600, Shimadzu, Japan) at the wavelength of 280nm, and the cumulative release curves for E2 were subsequently established.

Furthermore, due to the dynamic pH environment of human uteri, pH-sensitive E2 delivery behavior of M-N-(PDA@E2/HA)$_{20}$ scaffolds was investigated. M-N-(PDA@E2/HA)$_{20}$ scaffolds (3 samples for each pH) were immersed in different buffer solutions (at pH 4.5, pH 7.4, and pH 9.0) at 37℃, respectively. At predetermined time points, a small amount of immersion liquid was extracted, and an equal amount of fresh buffer solution was added. The amount of E2 released was similarly determined using the UV-vis spectrophotometer. As a result, the cumulative amount of E2 released in different buffer solutions was calculated, and E2 release curves were established.

2.7 *In vitro* biological evaluation

To evaluate the *in vitro* biological performance of different scaffolds (M, M-N, M-N-(PDA/HA)$_{20}$, and M-N-(PDA@E2/HA)$_{20}$ scaffolds), BMSCs obtained from healthy adult rats were used. The BMSCs were propagated in high-glucose Dulbecco's modified Eagle's medium (DMEM, Gibco) with 10% (v/v) fetal bovine serum (FBS, Gibco) and 1% (v/v) penicillin-streptomycin (Gibco). The cell culture work was performed in a CO_2 incubator supplemented with 5% CO_2 and 95% humidity at 37℃.

The cell attachment, viability, proliferation, and morphology of BMSCs on M-N-(PDA@E2/HA)$_{20}$ scaffolds were studied through, respectively, SEM observation, live/dead assay (Invitrogen, Thermo Fisher Scientific), MTT assay (Invitrogen, Thermo Fisher Scientific), and confocal laser scanning microscopy (CLSM) after phalloidin/DAPI staining (Invitrogen, Thermo Fisher Scientific). For cell adhesion experiment, BMSCs at the density of 5×10^4 cells per well were seeded on each sample (one sample per well) in a 24-well cell culture plate and cultured in DMEM at 37℃. After culturing for 24h, cells on scaffold samples were

immobilized using 4.0% paraformaldehyde for 30min in the dark. The immobilized cells on samples were then dehydrated using serial gradient ethanol solutions (50%, 60%, 70%, 80%, 90%, and 100%) for 10min each and then dried in the oven overnight. The dried samples with cells were sputtered with a thin layer of gold and the cell morphology on samples was observed under SEM.

For cell viability investigation, BMSCs at the density of 5×10^4 cells per well were seeded on samples (3 samples for each type of scaffolds) in the 24-well cell culture plate. After culturing for 24 and 48h, respectively, live/dead assay was used to stain the cells. Living cells were stained green and dead cells were stained red when observed under a fluorescence microscope (Leica DMi8, Germany). On the other hand, BMSCs at the density of 1×10^4 cells per well were seeded on scaffold samples (5 samples for each type of scaffolds) to study cell proliferation behavior and cell morphology. At predetermined time points (1, 3, and 7 days), cell proliferation was assessed using MTT assay. Meanwhile, on day 7 of culture, BMSCs cultured on scaffolds were visualized after phalloidin/DAPI staining under CLSM (Leica, Germany).

2.8 Fabrication of 3D bioprinted BMSC-laden hydrogel layer on M-N-(PDA@E2/HA)$_{20}$ scaffolds

2.8.1 GelMA synthesis and characterization

The synthesis of GelMA followed the previously established procedure [25]. Briefly, 10% (w/v) gelatin was dissolved in PBS under constant magnetic stirring at 60℃ in a water bath. Methacrylic anhydride (400μl per gram of gelatin) was added to the gelatin solution. The reaction was continued for 4h and then stopped by adding an equivalent volume of PBS. Subsequently, the solution was dialyzed against DI water at 40℃ for 7 days using dialysis tubes, with the DI water being changed daily. Finally, GelMA was obtained by freeze-drying and was stored at 4℃ until use. The degree of modification (DoM) of GelMA thus made was characterized using ^{1}H-NMR spectroscopy (Bruker Avance III 400, USA) and 2,4,6-Trinitrobenzenesulfonic acid (TNBS), respectively. An FT-IR spectrometer (PerkinElmer, USA) was also used to analyze the function groups of synthesized GelMA.

2.8.2 Rheological properties of GelMA/Gel bioinks

GelMA/Gel-based bioinks with incorporated BMSCs were made for 3D printing. In the current study, the rheological properties of GelMA/Gel bioinks were carefully studied. 5% (w/v) GelMA and 5% (w/v) Gel were dissolved in PBS under stirring at 50℃ in a water bath, with the 0.4% (v/v) photo-initiator being added in the solution. The rheological properties of GelMA/Gel bioinks were determined using a MCR 302 Rheometer (Anton Paar, Austria) equipped with a parallel plate unit of 25mm in diameter.

2.8.3 3D bioprinting of cell-laden hydrogel layer on M-N-(PDA@E2/HA)$_{20}$ scaffolds

GelMA/Gel bioinks containing BMSCs were used to fabricate a layer of cell-laden hydrogel onto M-N-(PDA@E2/HA)$_{20}$ scaffolds for mimicking of the structure and functions of the endometrium. In this study, GelMA/Gel solutions were mixed with BMSCs at room temperature to reach a final density of 1×10^6 cells per ml. The prepared bioinks were transferred to a cartridge in a 3D bioprinter (regenHU, Switzerland) for printing. The printing parameters were set as: the diameter of the printing nozzle was 210μm, the printing temperature was 20℃, and the printing speed was 6mm/s. After adjusting the initial height between the nozzle and scaffold, the bioinks were 3D printed on the surface of M-N-(PDA@E2/HA)$_{20}$ scaffolds. After 3D bioprinting, a UV light (360mW) was used to irradiate the structs of BMSC-laden GelMA/Gel scaffolds at the same speed as that for printing to crosslink the hydrogel structs (4 times, about 2min). Finally, the completed hierarchical scaffolds were transferred to 6-well cell culture plates supplemented with DMEM and cultured at 37℃.

2.9 Cell survival and shape morphing of uterine tissue scaffolds

For investigation the shape morphing ability of scaffolds, the complete, multilayered hierarchical scaffolds were immersed in the culture medium in a CO_2 incubator at 37℃ after 3D bioprinting. The shape morphing process was monitored and recorded by a digital camera. Furthermore, live/dead assay was used to study cell survival and cell distribution in the printed GelMA/Gel hydrogel layer under CLSM after the scaffolds evolved from their planar shape to the tubular structure. Also, after culturing for 1, 3, 5, and 7 days, respectively, the survival rates

of BMSCs in 3D printed cell-laden hydrogel were assessed.

2.10 Statistical analysis

The results presented in this article were obtained from at least 3 separate samples and were expressed as mean ± SD. One-way ANOVA was performed for statistical analysis. Statistically significant difference existed when: *$p<0.05$, **$p<0.01$, and ***$p<0.001$.

3. Results and discussion

3.1 Fabrication of M and M-N scaffolds

PLATMC [26] and PLGA [27] are popular biomaterials and are often used in tissue engineering and regenerative medicine because of their good biocompatibility and controllable biodegradation rates. Additionally, PLGA has already been used in investigations for uterine regeneration in rat or rabbit models [11]. For example, Chen *et al.* fabricated an E2 delivery system using PLGA microspheres as the vehicle for endometrium regeneration [28]. In the current study, to mimic the properties and biological functions of myometrium of human uterus, PLATMC with different LA:TMC ratios (9:1, 8:2, and 5:5) were mixed with PLGA at different PLATMC: PLGA ratios for fabricating M scaffolds. The mechanical properties of M scaffolds were studied using tensile tests (these data are not included in this article). It was found that when the ratio of PLATMC (LA:TMC = 8:2) : PLGA was 4:1, the M scaffolds produced would provide excellent mechanical properties while exhibiting satisfactory biological performance. However, as shown in Fig.S1, the surface roughness of M scaffolds was about 110nm, which was too flat for cell attachment and could impair the tissue regeneration process when the scaffolds were implanted in the body. Surface properties, especially surface morphology and wettability, play an important role in inducing cell polarization and modulating cell migration or even regulating gene expression and cell signaling pathways [29]. Patntirapong *et al.* showed that cell adhesion and proliferation increased with an increase in surface roughness [30]. However, some other studies suggested that a “smooth” surface would result in a better cell attachment, migration, and proliferation behavior than a rough surface [31, 32]. But these “smooth” surfaces were usually

at the micrometer level. Therefore, the surface of M scaffolds needed to be modified to increase its roughness and hence improve cellular response. Also, a very smooth surface is not conducive for constructing multilayer films on an M scaffold, i.e., for depositing PDA particles and HA polymer on the M scaffold in the current study.

Because PLATMC and PLGA are rich in ester moieties, NaOH etching is an easy way to modify their surface morphology through a hydrolysis reaction. A NaOH treatment could etch the surface of M scaffolds, resulting in increased surface roughness. Moreover, the cleavage of the ester bond would generate abundant -COOH and -OH groups on the surface of M scaffolds, causing the surface to be more hydrophilic, which would facilitate cell adhesion and proliferation. Previous studies had already demonstrated that a NaOH treatment could increase the surface roughness and wettability of PLA and PLGA scaffolds, thus improving their biocompatibility and bioactivity [33, 34]. Therefore, in the current study, a systemic investigation was conducted to look into the effects of NaOH concentration and etching time on the surface morphology and wettability of PLATMC/PLGA scaffolds. As shown in Fig.2A-C, with the increase in NaOH concentration or etching time, the surface of M-N scaffolds became rougher and the surface water contact angle decreased. Importantly, a high NaOH concentration and a long etching time would degrade PLATMC/PLGA scaffolds. According to the surface morphology visualized by SEM (Fig.2A), the surface morphology of M-N scaffolds was quantitively categorized into three groups (or, stages): rough, rounded, and degraded (Fig.2D). The rough surface morphology indicated that the scaffold surface was normal, while the rounded surface morphology suggested over-etching. In this context, PLATMC/PLGA scaffolds etched by 1.0M NaOH for 1.0h were considered to have a relatively good surface morphology and wettability. On the other hand, M-N scaffolds did not display lowered mechanical performance in comparison with M scaffolds (Fig. 5C). As a result, scaffolds etched by 1.0M NaOH for 1.0h would be used in subsequent studies. Their increased surface roughness would be beneficial for the construction of multilayer films. In the current study, the generation of -COOH and -OH on M-N scaffold surface would facilitate the fabrication of PDA@E2/HA multilayer films on these scaffolds.

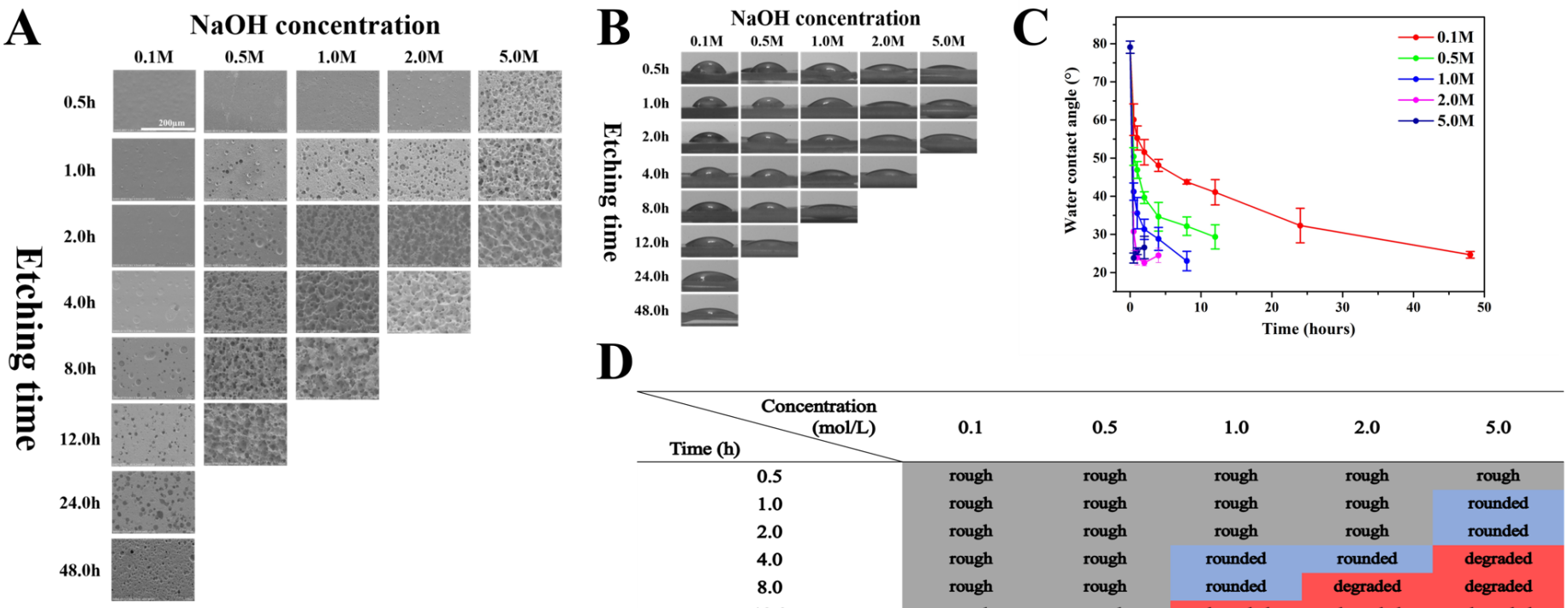

Time (h) \ Concentration (mol/L)	0.1	0.5	1.0	2.0	5.0
0.5	rough	rough	rough	rough	rough
1.0	rough	rough	rough	rough	rounded
2.0	rough	rough	rough	rough	rounded
4.0	rough	rough	rounded	rounded	degraded
8.0	rough	rough	rounded	degraded	degraded
12.0	rough	rough	degraded	degraded	degraded
24.0	rough	degraded	degraded	degraded	degraded
48.0	rough	degraded	degraded	degraded	degraded

Fig.2 Surface characteristics of M-N scaffolds after NaOH treatment. (A) Surface morphology of M-N scaffolds etched by NaOH solution of different NaOH concentrations (0.1, 0.5, 1.0, 2.0, and 5.0M) and for different time (0.5, 1.0, 2.0, 4.0, 8.0, 12.0, 24.0, and 48.0h). (B) Digital images of water contact angles of M-N scaffolds. (C) Relationships between M-N scaffold surface water contact angle and NaOH concentration and etching time. (D) Quantitative categorization of surface morphology of M-N scaffolds.

3.2 Synthesis and characterization of PDA and PDA@E2 particles

Inspired by the adhesive protein in mussels, applying dopamine in tissue engineering and regenerative medicine has been increasingly investigated [35]. Dopamine is a non-toxic and biocompatible material and is considered suitable for applications in tissue regeneration. Dopamine has the unique tethering ability to easily adhere to organic and inorganic surfaces via polymerization with the formation of PDA particles [36]. PDA particles have attracted great attention for tissue engineering and drug delivery applications due to their excellent adhesive properties, good biocompatibility, and biodegradability [37]. PDA particles can modify the substrate surface and hence improve cellular behavior, such as facilitating cell attachment and promoting cell proliferation. Zhang *et al.* fabricated PDA coating on electrospun silk fibroin scaffolds for promoting wound healing [38]. They found that the PDA coating layer could enhance the hydrophilicity and protein adsorption ability of silk fibroin scaffolds and the attachment, proliferation and spreading of fibroblasts. Notably, the application of PDA in drug delivery has also gained tremendous interest [22, 39]. PDA particles as drug carriers could provide controlled and sustained *in situ* drug delivery, thus prolonging the therapeutic effect. On the other hand, incorporating biomolecules in PDA particles could protect their bioactivity and maintain their effectiveness. Furthermore, drugs contained in PDA particles often display a smart release manner when the PDA particles are exposed to a suitable external stimulus. The release of drugs from PDA particles is usually sensitive to pH of the environment and near-infrared (NIR) laser irradiation [40]. For example, PDA particles showed to be an excellent vehicle for delivering doxorubicin (DOX), an anticancer drug, in anticancer therapies [41]. In the current study, PDA particles were used to encapsulate E2 and regulate E2 delivery behavior by modulating external stimuli such as pH and NIR laser irradiation, thus achieving the desired therapeutic effect in uterine tissue regeneration.

The main methods so far for biomolecule encapsulation in PDA particles can involve: (1) physical absorption of biomolecules by PDA via hydrogen bonding, electrostatic interaction, van der Waals's force, etc.; (2) chemical interaction of biomolecules on the outer face of PDA particles using chemical linkers; or (3) PDA-biomolecule conjugate formation [42]. However, using *in situ* polymerization to form biomolecule-loaded PDA particles would be an easy and

effective way in comparison with the three ways mentioned above. Importantly, the *in situ* polymerization method could provide a higher biomolecule loading efficiency than the aforementioned three ways. Therefore, in the current study, E2-loaded PDA particles were synthesized by *in situ* E2 loading via the polymerization of dopamine in a weak alkaline solution. Usually, E2 is poorly water-soluble. In the current study, an ethanol/water mixture was used to improve the solubility of E2. PDA@E2 particles were synthesized using different dopamine-to-E2 ratios. Noticeably, the maximum E2 solubility was reached when the dopamine-to-E2 ratio was 1:0.3. Overall, PDA@E2 particles were spherical in shape with an average diameter around 800-1,200nm (Fig.3). The incorporation of E2 in PDA particles did not significantly affect the particle morphology and diameter. Additionally, as shown in Fig.S2, PDA-0.1 particles had the highest E2 loading efficiency (about 83%), while PDA-0.2 and PDA-0.3 particles exhibited comparable loading efficiency (about 80%). In this context, PDA-0.3 particles were used for subsequent studies. Owing to its significant role in promoting angiogenesis and modulating endometrium regeneration, the application of E2 for uterine regeneration has already been investigated in preclinical and clinical trials [43, 44]. Generally, estrogen is orally administered [45]. However, because oral administration of estrogen lacks targetability, it normally results in low estrogen concentration at the injured endometrium sites due to the influence of the fluid circulation system. Incorporating E2 in PDA particles via *in situ* polymerization had increased the solubility and bioavailability of E2, which would help to enable estradiol delivery and provide sustained effect.

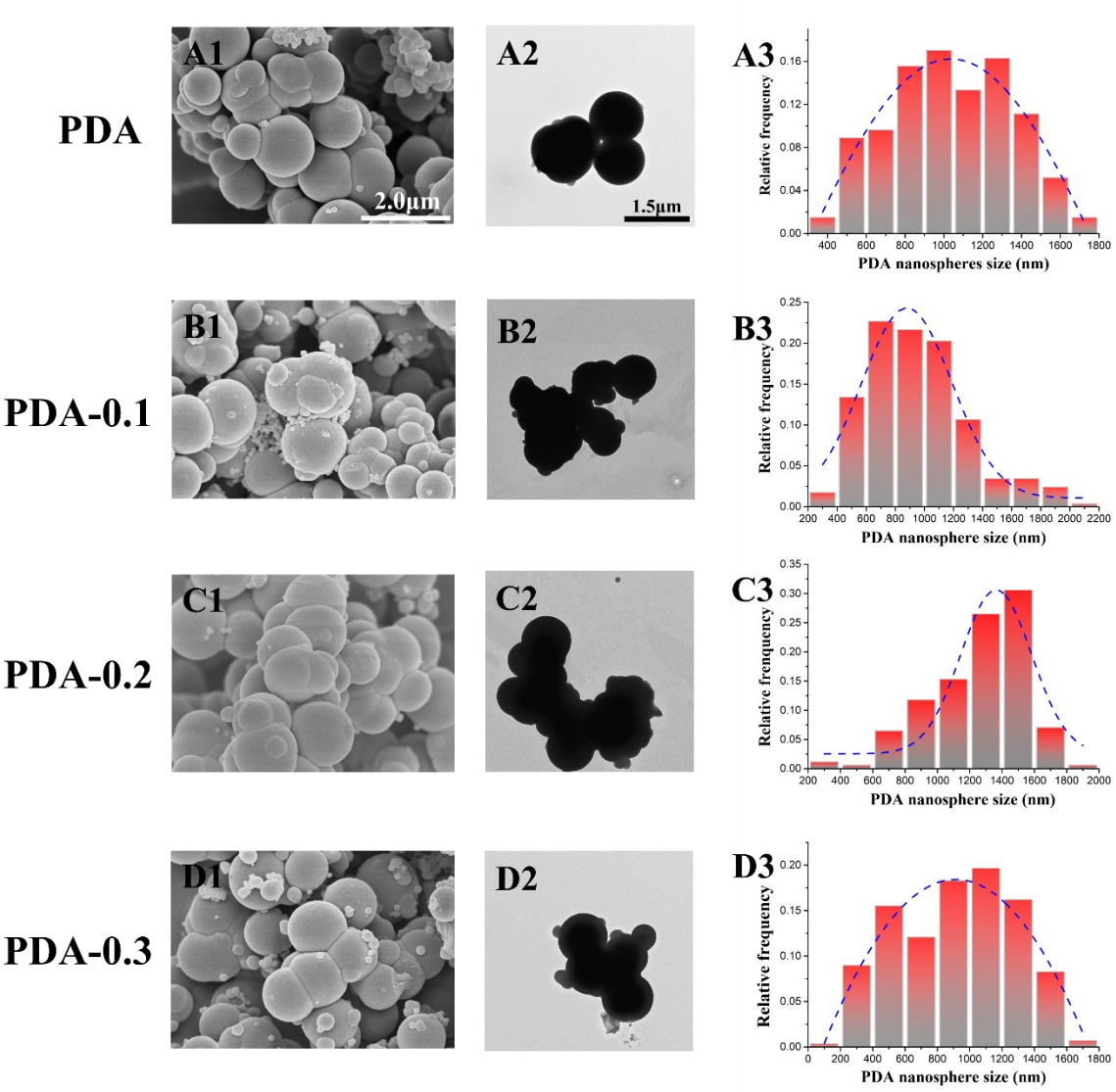

Fig.3 Morphology and size distribution of PDA and PDA@E2 particles. (A1-D1) SEM images of particles, (A2 to D2) TEM images of particles, and (A3 to D3) particle size distribution (PDA-to-E2 ratio: 1:0 for A1-A3, 1:0.1 for B1-B3, 1:0.2 for C1-C3, and 1:0.3 for D1-D3).

3.3 Construction of PDA@E2/HA multilayer films on M-N scaffolds

Using the layer-by-layer (LBL) self-assembly technique to construct multilayer films on 3D tissue engineering scaffolds is a versatile way to modify surface chemistry and properties and hence the performance of scaffolds, including improving surface hydrophilicity and guiding cell behavior [46, 47]. In addition, multilayer films could function as a drug delivery vehicle to

controllably and sustainably deliver the loaded drugs [48]. The LBL approach offers low cost, simplicity, versatility, and modularity for fabricating multilayer films on scaffold surface with tailored thickness, customized structure and desired properties. Therefore, applying the LBL technique to form multilayer films on scaffolds is often encountered in the tissue engineering and drug delivery fields [49, 50].

In the current study, PDA@E2 particles were paired with HA polymer to form multilayer films on the surface of M-N scaffolds for improving scaffold biological performance and for constructing E2 delivery platform to sustainably release E2, thus achieving sustained therapeutic effect of E2 and promoting uterine tissue regeneration. As mentioned in the previous section, M-N scaffolds were etched by a NaOH solution via surface hydrolysis, which led to the generation of abundant -COOH and -OH groups on the surface of M-N scaffolds. The presence of these reactive groups on M-N scaffolds made it easier to form the PDA@E2/HA multilayer films. Usually, multilayer films are fabricated via LBL self-assembly by a pair of polyelectrolytes: one cationic polyelectrolyte, and one anion polyelectrolyte. The sequential deposition of polyelectrolytes is mainly driven by electrostatic interaction, and other secondary interactions such as hydrogen bonding, coordination bonding, and biomolecular recognition are also involved [51]. PDA particles are positively charged. Therefore, in applying the LBL technique, PDA@E2 particles could be paired with negatively charged HA polymer to form multilayer films via the electrostatic force. Furthermore, PDA particles possess very adhesive properties due to their abundant catechol and amine groups [22]. Chemical reaction and hydrogen bonding were also involved in forming PDA@E2/HA multilayer films on M-N scaffolds. As shown in Fig.4A, SEM revealed the surface morphology of M-N scaffolds coated with $(PDA@E2/HA)_{10}$ and $(PDA@E2/HA)_{20}$ multilayer films, respectively. M-N scaffolds themselves displayed a very rough surface, while M-N-$(PDA@E2/HA)_{10}$ and M-N-$(PDA@E2/HA)_{20}$ scaffolds exhibited relatively smooth surfaces. Furthermore, PDA@E2 particles could be obviously seen on M-N-$(PDA@E2/HA)_{20}$ scaffolds. As illustrated by Fig.4B, it was found that when the PDA@E2/HA bilayer deposition number reached 3, the water contact angle became stable, which indicated that the PDA@E2/HA multilayer films had completely covered the scaffold surface. Cross-sectional views of the structures (Fig.4C) also

showed clearly the PDA@E2/HA multilayer films on the surface of M-N-$(PDA@E2/HA)_{10}$ and M-N-$(PDA@E2/HA)_{20}$ scaffolds, respectively. The visible presence of PDA@E2 particles in multilayer films is an evidence of the successful fabrication of PDA@E2/HA multilayer films on M-N scaffolds.

Different from other possible pairs of polyelectrolytes, the fabrication of multilayer films using PDA@E2 particles and HA polymer has combined the advantages of LBL assembly with unique properties of PDA-based particles. PDA@E2/HA multilayer films made from biocompatible and biodegradable PDA particles and HA polymer would significantly modify the surface of M-N scaffolds, including improving protein adsorption and cell response. In the current study, the formation of PDA@E2/HA multilayer films was mainly driven by electrostatic interaction and hence could be sensitive to the pH condition. Like most polyelectrolyte multilayer films, the H^+ and OH^- could influence the structure and integration of multilayer films and thus affect their drug release behavior [52]. Therefore, PDA@E2/HA multilayer films should exhibit a pH-responsive behavior. Previously, Hao *et al.* produced an intelligent PDA/sodium alginate (ALG) multilayer film for antifouling and antibacterial purposes [53]. The pH-responsive properties of their multilayer films enabled prolonged drug release, resulting in an extended period of antibacterial performance. On the other hand, PDA particles have proved to be a good photothermal agent [40]. Therefore, the release kinetics of E2 from PDA@E2/HA multilayer films may be regulated by NIR laser irradiation which could cause temperature increases of particles/films owing to the PDA in multilayer films. Consequently, the PDA@E2/HA multilayer films formed on M-N scaffolds would provide various benefits for uterine regeneration.

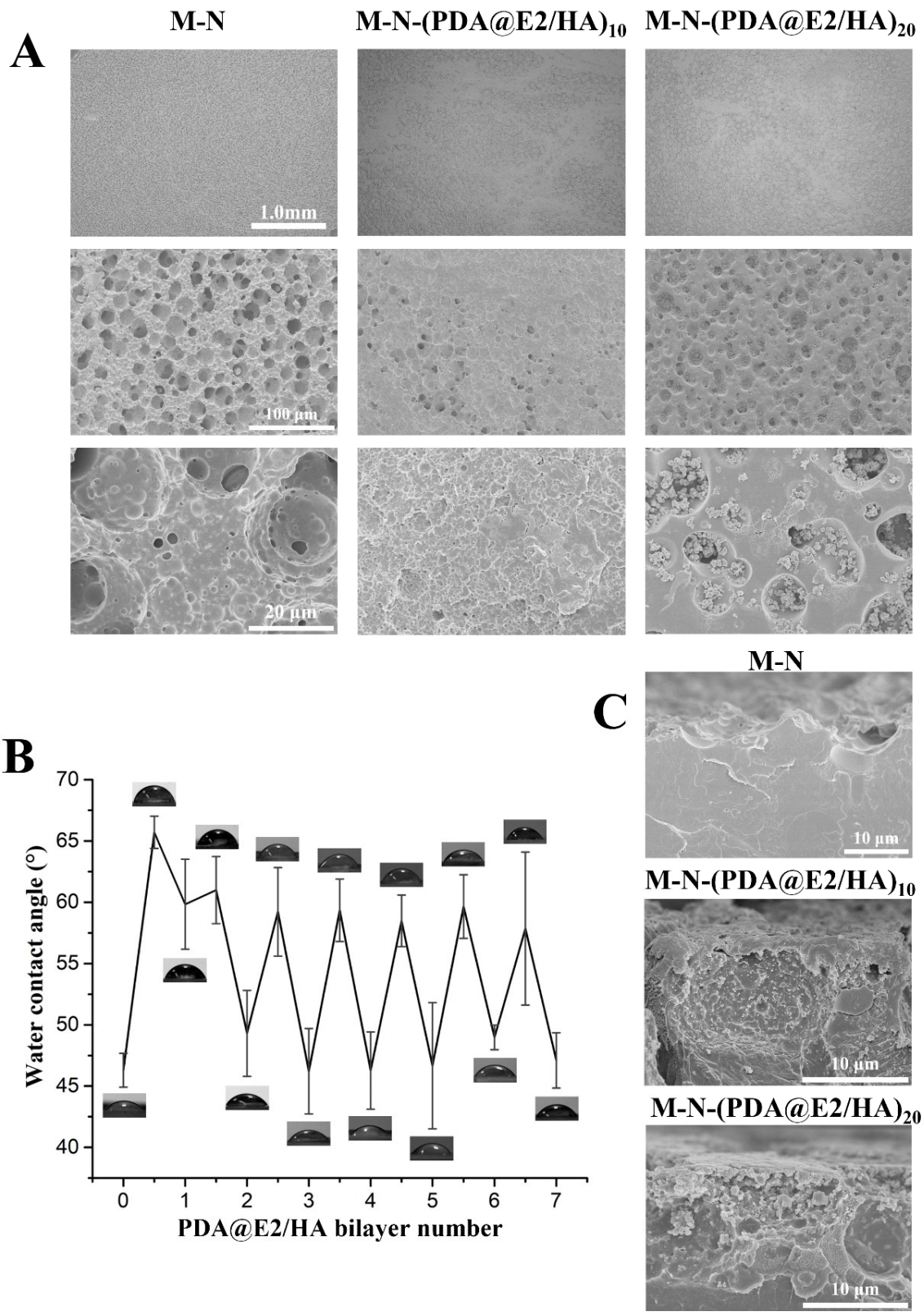

Fig.4 Characterization of PDA/HA multilayers on scaffolds. (A) SEM images showing the surface morphology of M-N, M-N-(PDA@E2/HA)$_{10}$, and M-N-(PDA@E2/HA)$_{20}$ scaffolds of different magnifications. (B) Variation of water contact angle of M-N

scaffold surface with the number of PDA@E2/HA bilayer film on the M-N scaffold. (C) Cross-sectional views of M-N, M-N-$(PDA@E2/HA)_{10}$, and M-N-$(PDA@E2/HA)_{20}$ scaffolds.

3.4 Mechanical properties of M-N-$(PDA@E2/HA)_{20}$ scaffolds

Human uterus is a myogenic organ, and myometrium having about 95% myocytes in volume is highly stretchable. What distinguishes uterus myocytes from myocytes in other smooth muscle tissues is their relatively large size. Therefore, smooth muscle cell-containing myometrium could tolerate contraction and expansion of the uterus for fetus development and parturition. Furthermore, myometrium supports stromal and vascular tissues.

In the current study, M-N scaffolds were improved by forming a PDA@E2/HA multilayer films on them, which would help to restore the functions of human uterus. As shown in Fig.5 and Table.S1, all scaffolds were highly stretchable. The elongation at break of M, M-N, M-N-$(PDA@E2/HA)_{10}$ and M-N-$(PDA@E2/HA)_{20}$ scaffolds was 514.01±11.13%, 501.42±29.99%, 498.20±17.42% and 501.37±22.98%, respectively, which are remarkable among all known tissue engineering scaffolds. There is no large difference for this property among the scaffolds. The ultimate tensile strength of M and M-N scaffolds was 0.83±0.12MPa and 0.89±0.06MPa, respectively. However, with the formation of PDA@E2/HA multilayer films on scaffolds, the tensile strength of M-N-$(PDA@E2/HA)_{10}$, and M-N-$(PDA@E2/HA)_{20}$ scaffolds increased to 1.49±0.08MPa and 1.62±0.12MPa, respectively. The PDA@E2/HA multilayer films on scaffolds had improved the strength and modulus of scaffolds but did not impair their elasticity (Fig.5D-5F). Previously, Manoogian *et al.* used uniaxial and biaxial testing methods to evaluate porcine and human uterine tissues [54, 55]. From their *ex vivo* studies, porcine uterine tissues showed peak stress of 320±176 kPa with a corresponding strain of 30±9.0%, while human uterus exhibited average peak stress of 656.3 ± 483.9 kPa with a corresponding strain of 32±11.2%. Moreover, from *in vivo* tests, human uterus could stretch to 110-130%. In the current study, M-N-$(PDA@E2/HA)_{20}$ scaffolds could stretch to 500% and their tensile strength was over 1.5MPa. Moreover, as shown in Fig.S3, M-N-$(PDA@E2/HA)_{20}$ scaffolds could

recover to the initial state within 20s after being stretched to 50% and 100% strain, respectively, suggesting the excellent elasticity of M-N-(PDA@E2/HA)$_{20}$ scaffolds. Furthermore, the deformation rate of scaffolds could be less than 10%. Therefore, the mechanical properties of M-N-(PDA@E2/HA)$_{20}$ scaffolds appear to be superior to native uterus, indicating significant advantages of these scaffold for uterine tissue regeneration.

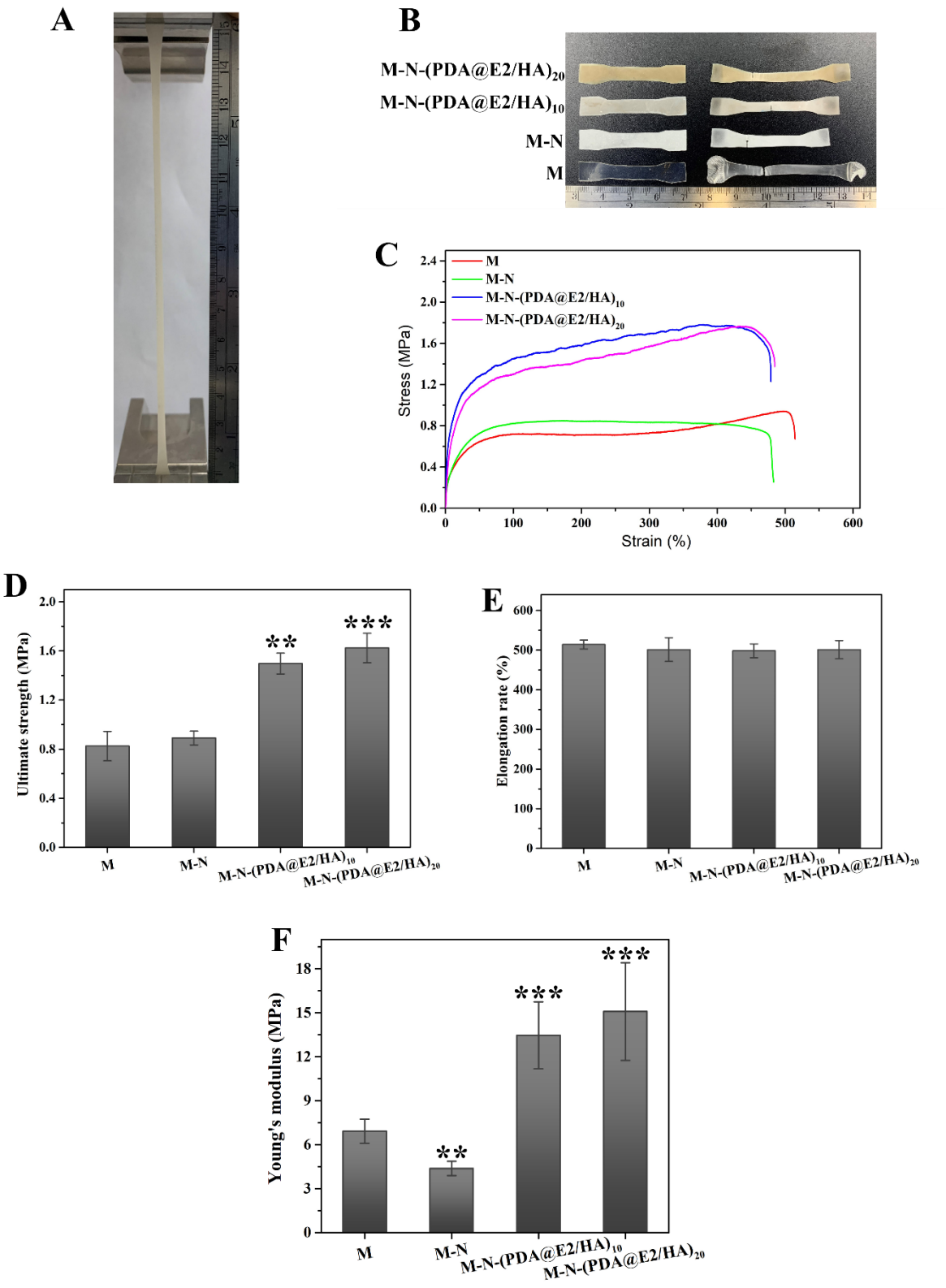

Fig.5 Mechanical behavior and properties of different scaffolds. (A) A photo showing an M-N-(PDA@E2/HA)$_{20}$ scaffold during tensile testing, (B) Scaffold samples before and after tensile tests, (C) Typical tensile stress-stain curves of scaffold samples, (D)

Ultimate tensile strength, (E) Elongation at break and (F) Young's modulus of M, M-N, M-N-(PDA@E2/HA)$_{10}$ and M-N-(PDA@E2/HA)$_{20}$ scaffolds.

3.5 Controlled and sustained release of E2 and biological properties of M-N-(PDA@E2/HA)$_n$ scaffolds

PDA particle is an excellent photothermal agent with good biocompatibility and biodegradability [56]. In the current study, the photothermal behavior of M-N-(PDA@E2/HA)$_{10}$ and M-N-(PDA@E2/HA)$_{20}$ scaffolds were investigated. Fig.6A-C show temperature changes of scaffolds when they were irradiated by an 808nm wavelength NIR laser at different energy densities (0.5 and 1.0 W/cm^2). Fig.S4 provides infrared thermal images of scaffolds under the irradiation of the NIR laser for different time. M-N-(PDA@E2/HA)$_{20}$ scaffolds could be heated up to 40℃ when irradiated at 1.0 W/cm^2 for 5min. To study the effect of NIR laser irradiation on E2 release, M-N-(PDA@E2/HA)$_{20}$ scaffolds were used. The E2 amount in the release medium was calculated based on the calibration curve, as illustrated by Fig.S5. Consequently, E2 release profiles, which could be regulated by NIR laser irradiation, were established (Fig.6D). It could be seen that with the NIR laser irradiation, more E2 was released from the scaffolds. The NIR laser irradiation obviously promoted E2 release from M-N-(PDA@E2/HA)$_{20}$ scaffold, which could be attributed to Brownian movements of drug molecules. The entropy as well as temperature of M-N-(PDA@E2/HA)$_{20}$ scaffolds was increased when irradiated by the NIR laser, thereby accelerating the movements of E2 molecules.

Since the pH value of uterine fluid is dynamics, experiments were conducted to study E2 release behavior in buffer solutions of different pH values (pH 4.5, 7.4 and 9.0). As shown in Fig.6E, the release of E2 from M-N-(PDA@E2/HA)$_{20}$ scaffolds could last for more than 28 days. This sustained E2 release would enable prolonged therapeutic effect and hence could facilitate uterine regeneration. Also, the E2 release kinetic could be depicted by the Higuchi model (Fig.S5D). Furthermore, it was seen that E2 could be quickly released in an alkaline environment and slowly in an acidic solution. This release behavior may be a result of the

PDA@E2/HA multilayer films. Generally, the electrostatic interaction between paired electrolytes could be interrupted by H^+ or OH^-, which would render the multilayer films pH-responsive [57]. Because PDA was positively charged and PDA-based particles could be readily disintegrated in alkaline solution, the interaction between PDA@E2 particles and HA polymer could be disturbed by OH^-. Consequently, a quick E2 release occurred in an alkaline solution.

Estrogen plays an essential role in regulating menstruation and endometrium regeneration for females [58]. The safety and efficacy of E2 delivery for endometrium regeneration have been confirmed in clinical studies [44, 45]. There are plentiful estrogen receptors on endometrium stromal cells and glandular epithelial cells. When E2 molecules bind to these receptors, they could perform their main function to promote the expression of angiogenic growth factors such as VEGF, bFGF and TGF-β1 [59]. Subsequently, those angiogenic growth factors would facilitate endothelial cell migration, proliferation, differentiation and tube formation and consequently increase blood vessel density and angiogenesis, thus improving the reconstruction of uterine tissues. However, as discussed earlier, E2 is poorly water-soluble and also has a limited half-life. The current practice of oral administration of E2 to treat uterine injury leads to very poor E2 availability at uterine injure sites. Therefore, a smart delivery vehicle should be formed to realize controlled and sustained E2 release *in situ* at the uterine injury sites. Several hydrogel systems were reported to encapsulate E2 for endometrium regeneration [60, 61]. In the current study, PDA@E2/HA multilayer films were constructed to deliver E2 *in situ* in a controlled manner. The results obtained have indicated that these films could provide controlled and sustained release of E2. In addition, it was found that the E2 release speed was associated with NIR laser irradiation and solution pH value. The pH value in the uterine cavity is not constant and varies according to the female health condition and menstruation. Therefore, apart from pH-responsive delivery of E2, the E2 release speed would be controlled by changing the NIR laser irradiation time and density, thereby promoting uterine regeneration.

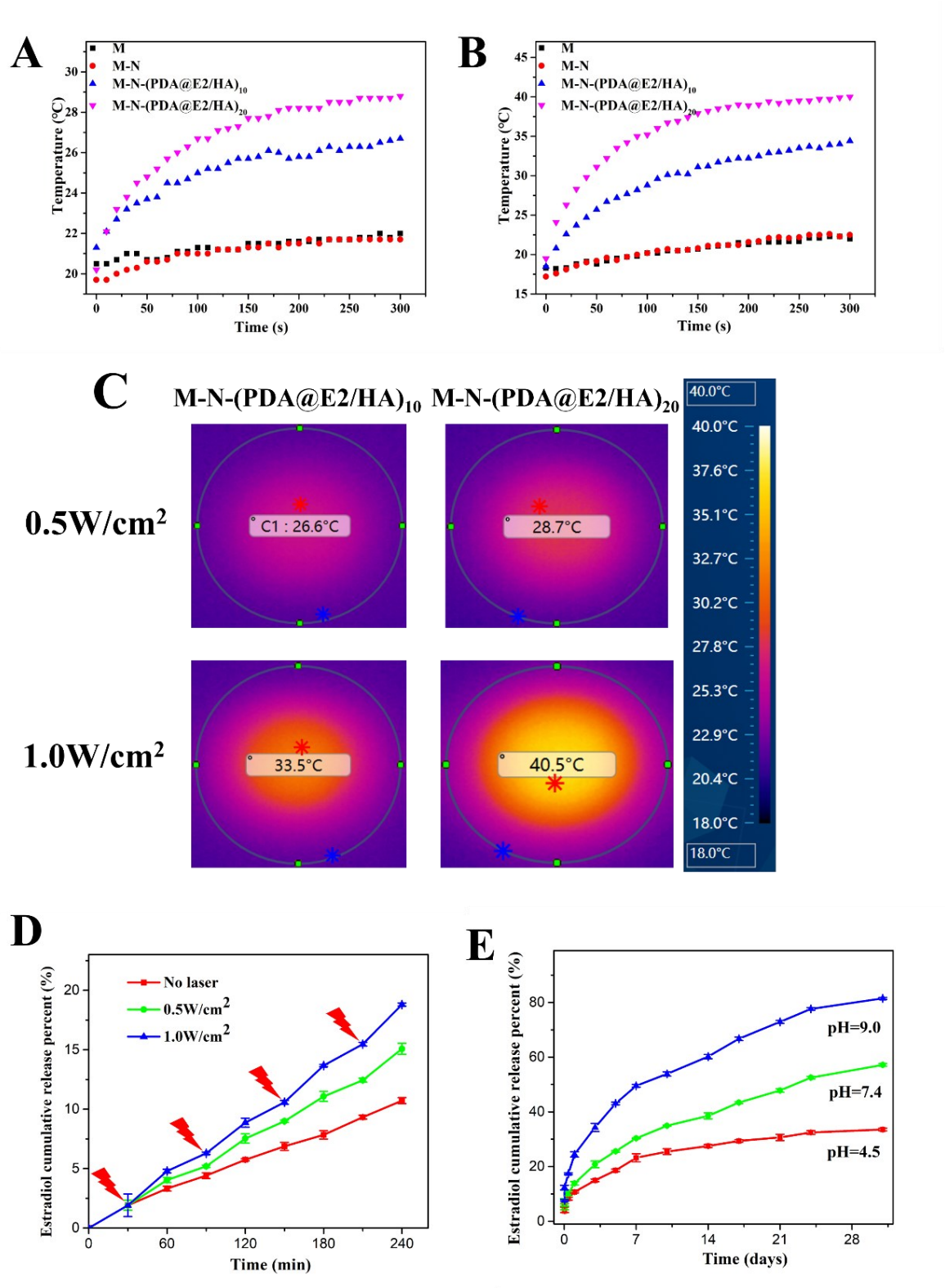

Fig.6 Photothermal effect and controlled E2 release from different scaffolds. Temperature changes of M, M-N, M-N-(PDA@E2/HA)$_{10}$ and M-N-(PDA@E2/HA)$_{20}$ scaffolds under the irradiation of an 808nm wavelength NIR laser at the power density of (A) 0.5 W/cm^2 and (B) 1.0 W/cm^2. (C) Infrared thermal images of M-N-(PDA@E2/HA)$_{10}$

and M-N-(PDA@E2/HA)$_{20}$ scaffolds for a 5-min NIR laser irradiation. (D) *In vitro* E2 cumulative release from M-N-(PDA@E2/HA)$_{20}$ scaffolds with or without NIR irradiation (at 0.5 and 1.0 W/cm^2, respectively) in PBS (pH 7.4). (E) *In vitro* E2 cumulative release of M-N-(PDA@E2/HA)$_{20}$ scaffolds in buffer solutions of pH 4.5, pH 7.4, and pH 9.0, respectively.

In vitro and *in vivo* studies have shown that BMSCs could directly differentiate into endometrium epithelial cells to improve gland and blood vessel formation, thereby promoting endometrium regeneration [62]. BMSCs could also stimulate and activate the resident endometrium stem cells to promote uterine regeneration via the paracrine effect. Therefore, in the current study, BMSCs were used to evaluate *in vitro* biological performance of scaffolds fabricated. It was found that scaffolds coated with PDA@E2/HA multilayer films exhibited a relatively higher BSA adsorption than M and M-N scaffolds, as shown in Fig.S6. Furthermore, among all scaffolds tested, M-N-(PDA@E2/HA)$_{20}$ scaffolds showed the highest BMSC proliferation rate (Fig.7C), which suggested that PDA@E2/HA multilayer films were beneficial for cell growth. The live/dead assay results indicated that M, M-N, M-N-(PDA/HA)$_{20}$, and M-N-(PDA@E2/HA)$_{20}$ scaffolds were all highly biocompatible. The cell survival rates of BMSCs on the scaffolds were all higher than 95%, and there was no significant difference among these scaffolds (Fig.7A, B). The cell morphology and internal structure of BMSCs cultured on different scaffolds were studied using SEM and CLSM after phalloidin/DAPI staining. SEM observations showed that BMSCs exhibited well-spread morphology on scaffolds (Fig.S7), and CLSM images revealed that BMSCs had spindle-like morphology and maintained their phenotype on scaffolds (Fig.7D). Overall, the M-N-(PDA@E2/HA)$_{20}$ scaffolds showed the best *in vitro* biological performance and could promote BMSC growth and proliferation.

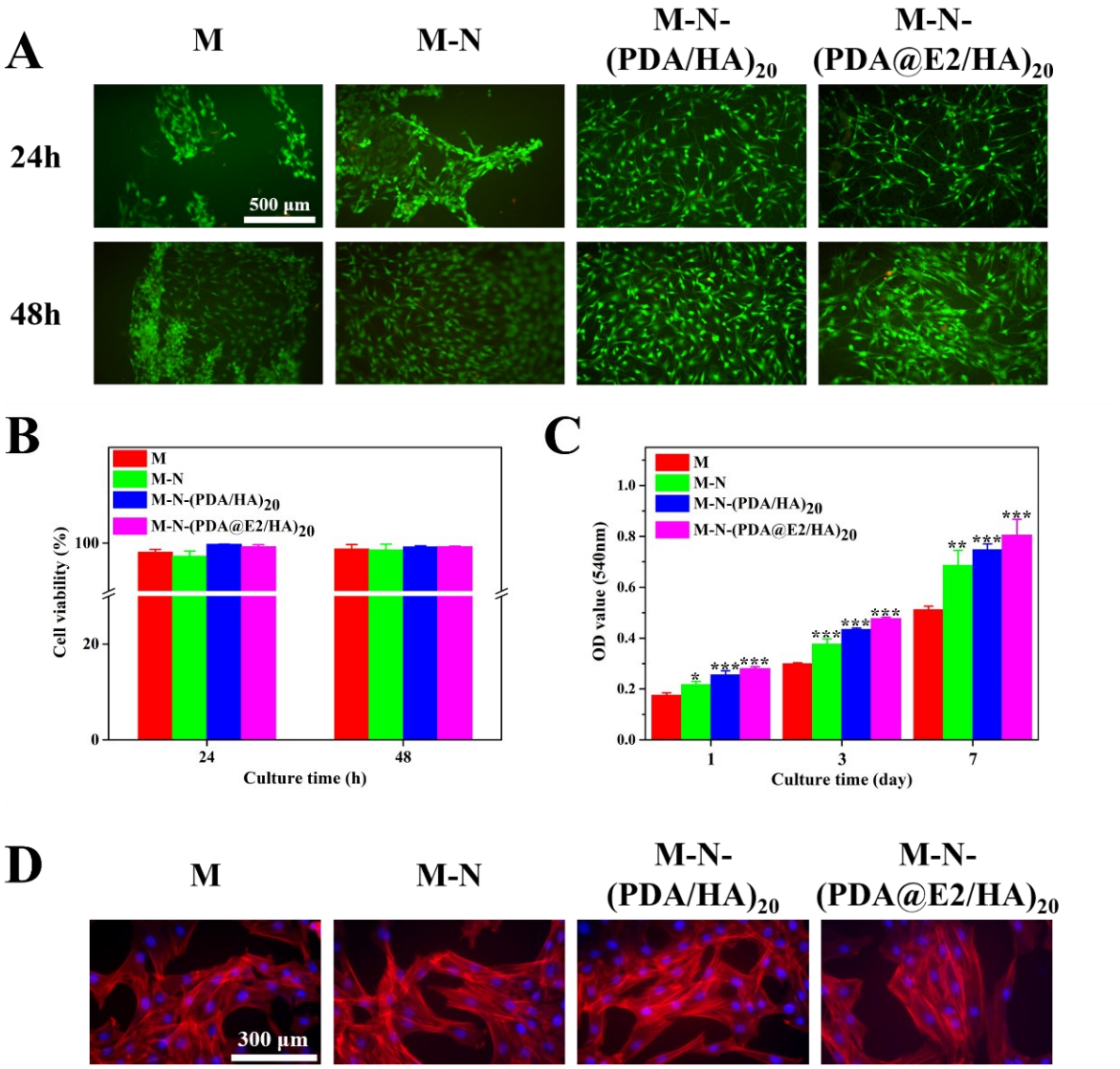

Fig.7 *In vitro* biological performance of different scaffolds. (A) Fluorescence images of BMSCs cultured on M, M-N, M-N-(PDA/HA)$_{20}$ and M-N-(PDA@E2/HA)$_{20}$ scaffolds for 24h and 48h, respectively. (Live cells were stained green and dead cells were stained red.) (B) Cell survival rates of BMSCs cultured on M, M-N, M-N-(PDA/HA)$_{20}$ and M-N-(PDA@E2/HA)$_{20}$ scaffolds. (C) Cell proliferation of BMSCs cultured on M, M-N, M-N-(PDA/HA)$_{20}$ and M-N-(PDA@E2/HA)$_{20}$ scaffolds. (D) CLSM images showing nucleus and F-actin (blue for nucleus and red for F-actin) of BMSCs cultured on M, M-N, M-N-(PDA/HA)$_{20}$ and M-N-(PDA@E2/HA)$_{20}$ scaffolds for 7 days.

3.6 Fabrication and properties of hierarchical structured tissue engineering scaffolds for uterine regeneration

Although M-N scaffolds coated with the PDA@E2/HA multilayer films could provide a controlled and sustained E2 release and exhibited excellent *in vitro* biological performance, constructing a layer of cell-laden hydrogel on the surface of these scaffolds to mimic the multilayer and hierarchical structure of the native uterine tissue should be more beneficial for uterine regeneration. Bioinks involving Gel and GelMA have been widely used to fabricate cell-laden hydrogel scaffolds via 3D bioprinting for tissue engineering applications [63, 64]. Stem cell-laden 3D printed Gel or GelMA scaffolds could provide abundant autologous stem cells at tissue regeneration sites. Those stem cells would secrete matrix proteins to establish extracellular matrix (ECM) and attract surrounding cells to migrate towards the regeneration sites via auto-/paracrine effect, thus facilitating tissue remodeling. Also, attempts have been made to utilize Gel and GelMA to repair endometrium injury in recent years. For example, due to the arginine-glycine-aspartic (RGD) motifs in gelatin chains and because of less antigenic and immunological response in comparison with collagen, Gel and GelMA hydrogels were shown to promote angiogenesis and support endometrium endothelial cell tube formation and endometrium stromal cell growth in uterine regeneration [65, 66]. In the current study, according to our design, 3D printing of BMSC-laden GelMA/Gel hydrogel on the surface of M-N-$(PDA@E2/HA)_{20}$ scaffolds was conducted to form the final, hierarchical structured scaffolds for uterine regeneration.

Firstly, GelMA was synthesized per established protocol [25]. As can been seen in Fig.S8, the FT-IR spectrum for synthesized GelMA showed that the introduction of the small moiety -O-CH2-CH=CH2 into Gel chains caused the redshift of N-H vibration. Moreover, the amide characteristic peaks of GelMA, amide I ($1632cm^{-1}$) and amide II ($1538cm^{-1}$) were more prominent than those shown in Gel chains because of the addition of the methacrylate group. The ^{1}H-NMR spectrum for synthesized GelMA revealed the presence of new peaks around 6.00-5.86ppm (m, -O-CH2-CH=CH2) and 5.38-5.22ppm (t, -O-CH2-CH=CH2). The DoM of the GelMA was calculated to be about 80.6%. After GelMA synthesis, GelMA/Gel blend inks were prepared. The GelMA/Gel inks showed an excellent shear-thinning phenomenon,

indicating their potentially good printability for 3D printing (Fig.8A). Furthermore, the rheological study of GelMA/Gel inks indicated that these inks existed in the gel state at both 25 and 37℃ after being UV crosslinked for 2min (Fig.8B and 8C), indicating the good photocurable ability of GelMA/Gel inks.

The suitable rheological properties of GelMA/Gel inks implied their feasible use for 3D bioprinting. Therefore, BMSCs were added to GelMA/Gel blends to form bioinks for the fabrication of the cell-laden hydrogel layer on M-N-(PDA@E2/HA)$_{20}$ scaffolds via 3D bioprinting. The cell viability in the 3D printed hydrogel layer was evaluated using live/dead assay and the results are presented as Fig.9A and 9B. As the culture time increased, the GelMA/Gel hydrogel layer degraded gradually and encapsulated BMSCs could spread gradually and were eventually released from the scaffolds. Generally, 3D printed stem cell-laden hydrogel scaffolds can introduce autologous stem cells in implantation sites and these cells secrete various cytokines, growth factors, proteins, etc., that promote tissue regeneration. Since BMSCs had been shown to be beneficial for endometrium regeneration, in the current study, the BMSC-laden GelMA/Gel hydrogel printed on M-N-(PDA@E2/HA)$_{20}$ scaffolds could release abundant BMSCs at tissue regeneration sites, which would facilitate uterine regeneration through auto-/paracrine effect. The live/dead assay results showed that BMSCs had the highest cell survival rate (about 98%) at day 0. After culturing for 1 day, the cell survival rate decreased to 86.5% on M-N-(PDA/HA)$_{20}$ scaffolds and 85.6% on M-N-(PDA@E2/HA)$_{20}$ scaffolds. But it recovered to 96% on day 7 of culture. These results suggested that it could be advantageous to use BMSC-laden GelMA/Gel hydrogel coated M-N-(PDA@E2/HA)$_{20}$ scaffolds for uterine regeneration.

Human uterus has a complex, hierarchical structure in the curved shape. Although flat multilayered scaffolds which mimicked the structure and functions of the uterus may be made for use, as has been shown in the current study, ideally, the scaffolds should be in tubular or curved shape for fitting into the injured/damaged uterus. Scaffolds with a shape morphing ability to transform from planar structures to curved or tubular structures upon suitable stimulus/stimuli would be advantageous for uterine tissue engineering. Shape morphing upon receipt of a stimulus provides feasible a way for the fabrication of curved or tubular scaffolds

with hierarchical structures [67, 68]. With reference to the 4D printing principle, based on a PLATMC/PLGA substrate of a suitable glass transition temperature (Tg) (Fig.S9), the multilayered scaffolds produced in the current study could keep their planar shape at room temperature and would evolve completely into the tubular shape at 37℃. Video.S1 shows the whole shape morphing process of the final scaffold, while Fig.S10 displays the tubular shape of M, M-N and M-N-(PDA@E2/HA)$_{20}$ scaffolds after transformation from the original planar shape. The shape morphing behavior of these scaffolds could be attributed to the amorphous nature of the PLATMC polymer in the scaffolds. M scaffolds were shaped into tubular structures using a stainless steel rod at 50℃. The gradient increase in temperature from the surface to interior during the heating process affected the degree of molecular orientation, thereby resulting in anisotropic birefringence and inhomogeneous transparency. For the subsequently flattened scaffolds, the memory of the tubular shape was already built in in the flat scaffolds. When cultured in a physiological environment at 37℃, flat scaffolds were heated up and glass transition took place, causing the flat scaffolds to transform into curved or tubular structures. For a good visualization of the 3D bioprinted hydrogel layer on M-N-(PDA@E2/HA)$_{20}$ scaffolds, in a set of experiments, a blue dye was added in GelMA/Gel-based bioinks before 3D bioprinting. Fig.9C shows the final structure of a multilayered, hierarchical structured tissue engineering scaffold containing a BMSC-laden GelMA/Gel hydrogel layer (which was in blue color) on the surface. Owing to the shape morphing ability, this tissue engineering scaffold with a hierarchical structure was in the tubular shape at 37℃, mimicking the innate structure of the uterine tissue. Moreover, the final tissue engineering scaffolds exhibited superior mechanical properties and could provide controlled and sustained E2 release at the injury/damage sites after implantation, which would make the scaffolds a good graft for uterine defects. In addition, the BMSC distribution inside the hydrogel layer of the scaffold was revealed by CLSM imaging (Fig.9D). BMSCs were found to be homogeneously distributed in the hydrogel layer of the final tissue engineering scaffolds. Also, even after shape morphing into the tubular structure at 37℃, BMSCs in 3D printed GelMA/Gel hydrogel layer exhibited a very high survival rate.

On the other hand, the multilayer-structured scaffolds thus produced would exhibit unique

degradation behavior. Fig.9A has displayed the initial degradation of scaffolds. Like other cell-laden hydrogels [69], in the *in vitro* or *in vivo* environment, the BMSC-laden hydrogel layer of multilayered scaffolds would be degraded in weeks and hence would release encapsulated BMSCs gradually into the surrounding environment. Moreover, the PDA@E2/HA multilayer-film scaffold layer would disintegrate in months because of the enzymatic and pH microenvironment. Finally, as shown by other studies [26], biodegradation of the PLATMC/PLGA scaffold layer would last for years. In our subsequent studies, the biodegradation behaviour, mechanism and kinetics will be investigated for the multilayered scaffolds and consequently, the multilayer structure of scaffolds could be fine-tuned. In our current study, the emphasis was on designing, fabricating and characterizing trilayer scaffolds that mimicked the uterine tissue. In the next stage of research, more *in vitro* differentiation experiments and *in vivo* animal investigations will also be conducted to examine the safety and efficacy of our trilayer scaffolds on uterine tissue regeneration. These studies will help to gain more insights into multilayered scaffolds and assist the development of this type of biomimicking scaffolds for uterine tissue regeneration.

As has been shown in this article, the novelty of our current study includes (1) applying 4D printing in uterine tissue engineering, (2) designing and fabricating via 4D printing multilayered biomimicking scaffolds for regenerating both endometrium and myometrium of the uterine tissue, and (3) combining stem cell delivery and E2 release for effective uterine tissue regeneration. It has been demonstrated through current study that 4D printing and bioprinting are powerful for creating novel scaffolds for uterine tissue regeneration.

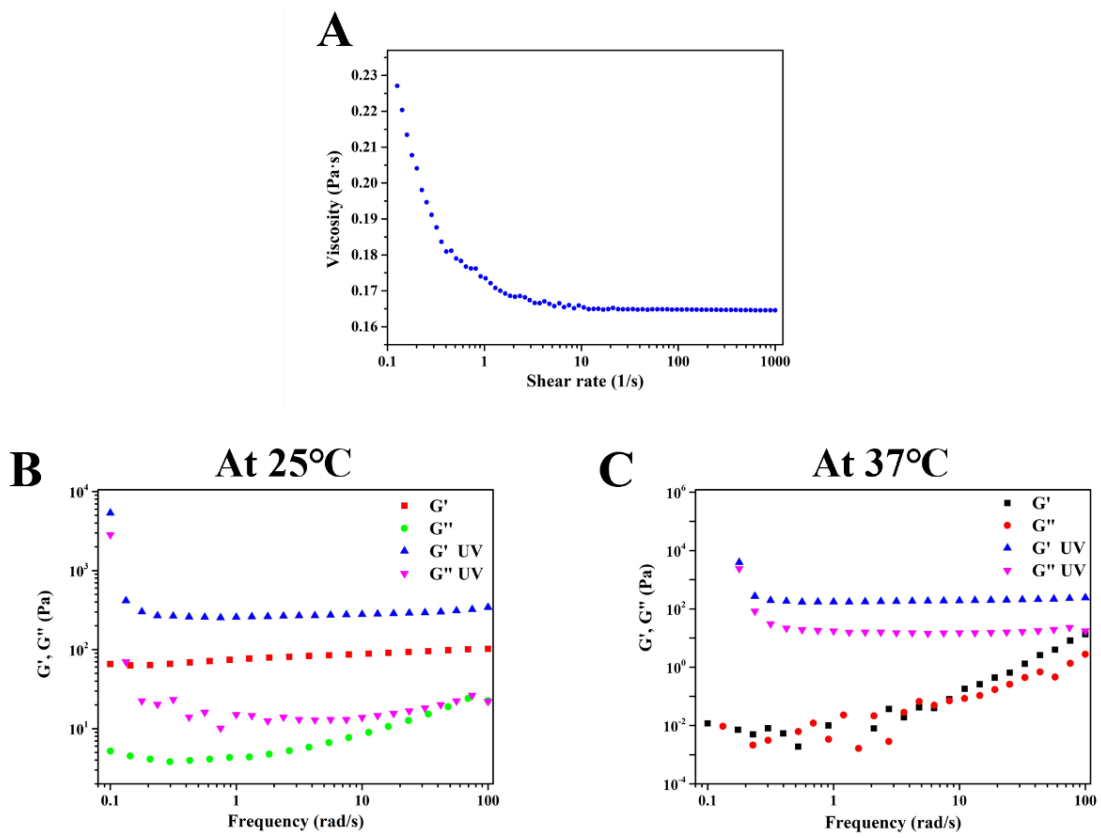

Fig.8 Rheological properties of 3D printing GelMA/Gel inks. (A) Shear thinning behavior of a GelMA/Gel ink. Rheological properties of UV crosslinked inks at (B) 25℃ and (C) 37℃.

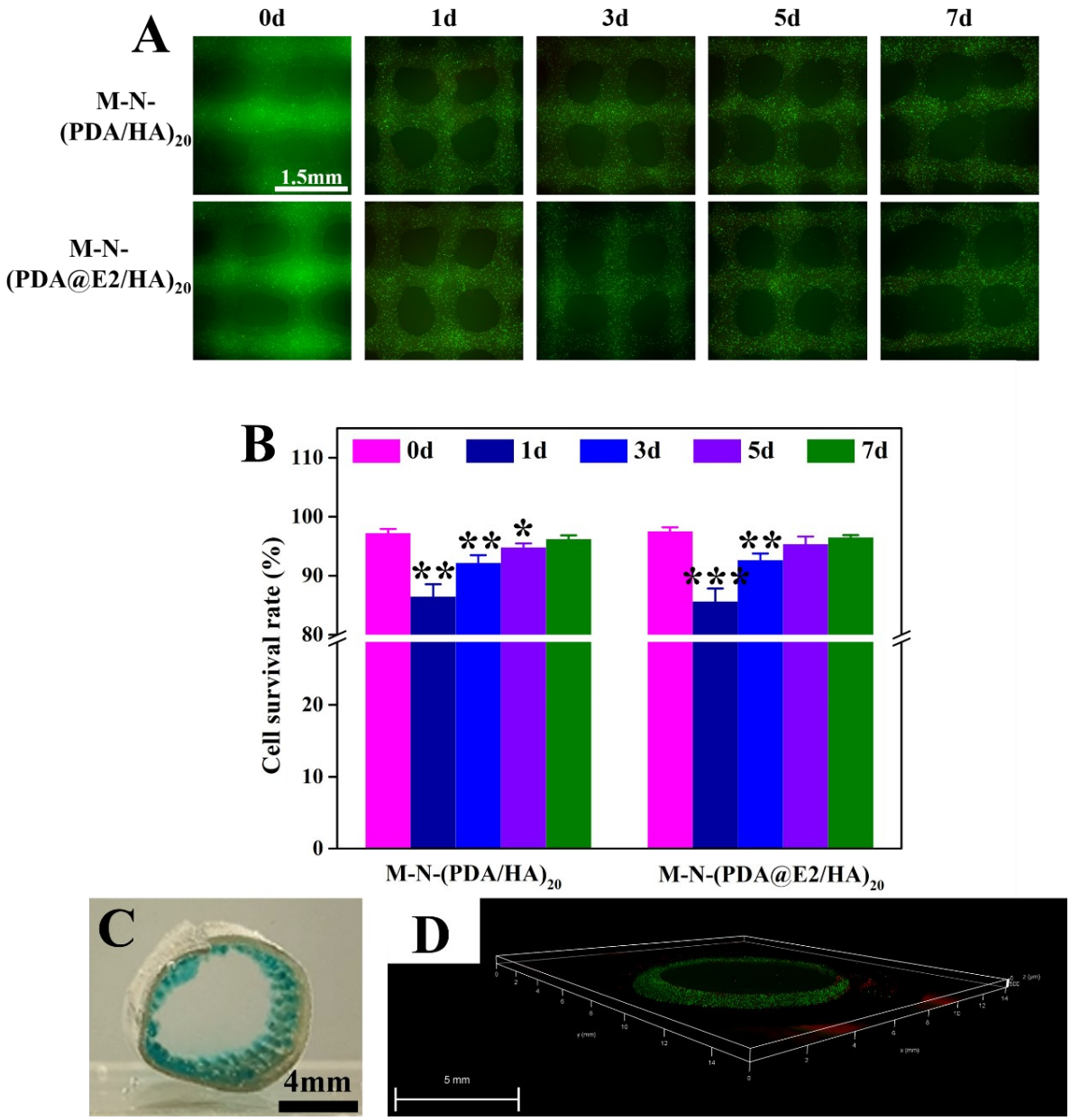

Fig.9 3D printed cell-laden GelMA/Gel hydrogel and hierarchical structured tissue engineering scaffolds for uterine tissue regeneration. (A) Live/dead assay results of 3D printed BMSC-laden hydrogel on M-N-(PDA/HA)$_{20}$ and M-N-(PDA@E2/HA)$_{20}$ scaffolds, respectively. (B) Cell survival rates of BMSCs in 3D bioprinted cell-laden hydrogel on M-N-(PDA/HA)$_{20}$ and M-N-(PDA@E2/HA)$_{20}$ scaffolds, respectively. (C) A photo showing a shape-morphed (self-folded), hierarchical structured scaffold. (A blue dye was used for visualizing the cell-laden hydrogel layer on the M-N-(PDA@E2/HA)$_{20}$ layer of the scaffold.) (D) A CLSM image showing the distribution

of BMSCs in the GelMA/Gel hydrogel layer of a hierarchical structured scaffold after the flat scaffold self-folded into the tubular shape after being immersed in the culture medium at 37℃.

4. Conclusions

In the current study, a multilayered and hierarchical structured tissue engineering scaffold mimicking the structure and functions of uterine tissue was designed and scaffolds of this design were successfully fabricated via solvent casting, layer-by-layer self-assembly, and 3D bioprinting. The final tissue engineering scaffolds had three distinctive layers: PLATMC/PLGA structural layer, PDA@E2/HA multilayer films layer, and BMSC-laden GelMA/Gel hydrogel layer. PDA@E2/HA multilayer films formed on PLATMC/PLGA scaffolds improved the mechanical properties, making the tissue engineering scaffolds superior to the uterine tissue. Additionally, the PDA@E2/HA multilayer film layer could provide controlled and sustained release of E2. Also, E2 release was pH-responsive and could be controlled by NIR laser irradiation. Furthermore, BMSCs exhibited a very high survival rate and a homogeneous distribution in the 3D bioprinted GelMA/Gel hydrogel layer of tissue engineering scaffolds. The cells could gradually spread and would be released from GelMA/Gel hydrogel. Importantly, the tissue engineering scaffold had the shape morphing ability to form curved or tubular structures when cultured at physiological environment at 37℃. The final tissue engineering scaffolds constructed in the current study had the multilayered and hierarchical structure as that of the uterine tissue, exhibited high stretchability, and provided controlled and sustained E2 release, which would make them very promising for uterine tissue regeneration.

Supporting information

Fig.S1 Surface morphology of M scaffolds. (A) and (B) SEM images of M scaffolds. (C) Atomic force microscope (AFM) image of an M scaffold.

Fig.S2 E2 loading efficiency of PDA particles with different dopamine to E2 ratios.

Fig.S3 Recovery of M-N-(PDA@E2/HA)$_{20}$ scaffolds after stretching to (A) 50% strain and (B) 100% strain, respectively.

Fig.S4 Infrared thermal images of M, M-N, M-N-(PDA@E2/HA)$_{10}$, and M-N-(PDA@E2/HA)$_{20}$ scaffolds under the irradiation of an 808nm wavelength NIR laser at the power density of 1.0 W/cm^2 for different times.

Fig.S5 (A) and (B) Optical density (OD) values of solutions of different E2 concentrations as measured by a UV-vis spectrometer. (C) Calibration curve for OD values (at 280nm wavelength) and E2 concentrations. (D) Application of the Higuchi model for E2 release from M-N-(PDA@E2/HA)$_{20}$ scaffolds.

Fig.S6 BSA absorption by M, M-N, M-N-(PDA@E2/HA)$_{10}$, and M-N-(PDA@E2/HA)$_{20}$ scaffolds.

Fig.S7 SEM images showing the morphology of BMSCs cultured on (A1, A2) M, (B1, B2) M-N, (C1, C2) M-N-(PDA/HA)$_{20}$, and (D1, D2) M-N-(PDA@E2/HA)$_{20}$ scaffolds.

Fig.S8 Characteristics of synthesized GelMA and Gel. (A) FT-IR spectra, (B) ^{1}H-NMR spectra.

Fig.S9 DSC curves for PLATMC, PLGA and PLATMC/PLGA.

Fig.S10 Tubular structures of M, M-N, and M-N-(PDA@E2/HA)$_{20}$ scaffolds evolved from the original planar shape after being immersed in a 37℃ water bath.

Table.S1 Tensile properties of M, M-N, M-N-(PDA@E2/HA)$_{10}$, and M-N-(PDA@E2/HA)$_{20}$ scaffolds.

Video.S1 The shape morphing process of the final tissue engineering scaffold.

Author Contribution Statement

Shangsi Chen: design of the research, methodology, investigation, writing, revision; Shenglong Tan: methodology, investigation, reviewing, revision; Liwu Zheng: reviewing, editing; Min Wang: design of the research, research supervision, writing, reviewing, revision, editing.

Conflict of Interest Statement

There are no conflicts of interest to declare.

Acknowledgments

M. Wang thanks Hong Kong's Research Grants Council (RGC) for the financial support for this work through research grants 17200519, 17202921, 17201622 and N_HKU749/22 and also The University of Hong Kong (HKU) through research grants in its Seed Fund for Basic Research Scheme. S. Chen thanks HKU for providing him with a PhD scholarship. Assistance provided by members of M. Wang's research group and by technical staff in HKU's Department of Mechanical Engineering, Faculty of Dentistry and Electron Microscopy Unit is acknowledged.

Reference

1. Zegers-Hochschild, F.; Adamson, G. D.; de Mouzon, J.; Ishihara, O.; Mansour, R.; Nygren, K.; Sullivan, E.; Vanderpoel, S.; International Committee for Monitoring Assisted Reproductive, T.; World Health, O., International Committee for Monitoring Assisted Reproductive Technology (ICMART) and the World Health Organization (WHO) revised glossary of ART terminology, 2009. *Fertility and Sterility* **2009,** *92* (5), 1520-1524.
2. Kisu, I.; Banno, K.; Mihara, M.; Suganuma, N.; Aoki, D., Current Status of Uterus Transplantation in Primates and Issues for Clinical Application. *Fertility and Sterility* **2013,** *100* (1), 280-294.
3. Johannesson, L.; Richards, E.; Reddy, V.; Walter, J.; Olthoff, K.; Quintini, C.; Tzakis, A.; Latif, N.; Porrett, P.; O'Neill, K.; Testa, G., The First 5 Years of Uterus Transplant in the US: A Report From the United States Uterus Transplant Consortium. *JAMA Surgery* **2022,** *157* (9), 790-797.
4. Brännström, M.; Johannesson, L.; Bokström, H.; Kvarnström, N.; Mölne, J.; Dahm-Kähler, P.; Enskog, A.; Milenkovic, M.; Ekberg, J.; Diaz-Garcia, C.; Gäbel, M., Livebirth After Uterus Transplantation. *The Lancet* **2015,** *385* (9968), 607-616.
5. Brannstrom, M.; Racowsky, C.; Carbonnel, M.; Wu, J.; Gargiulo, A.; Adashi, E. Y.; Ayoubi, J. M., Uterus Transplantation: from Research, through Human Trials and into the Future. *Human Reproduction Update* **2023**.
6. Liu, X.; Wu, K.; Gao, L.; Wang, L.; Shi, X., Biomaterial Strategies for the Application of Reproductive Tissue Engineering. *Bioactive Materials* **2022,** *14*, 86-96.
7. Li, X.; Lv, H. F.; Zhao, R.; Ying, M. F.; Samuriwo, A. T.; Zhao, Y. Z., Recent Developments in Bio-scaffold Materials as Delivery Strategies for Therapeutics for Endometrium Regeneration. *Mater Today Bio* **2021,** *11*, 100101.
8. Almeida, G. H. D.; Iglesia, R. P.; Araujo, M. S.; Carreira, A. C. O.; Santos, E. X. D.; Calomeno, C.; Miglino, M. A., Uterine Tissue Engineering: Where We Stand and the Challenges Ahead. *Tissue Engineering Part B: Reviews* **2022,** *28* (4), 861-890.
9. Li, X.; Sun, H.; Lin, N.; Hou, X.; Wang, J.; Zhou, B.; Xu, P.; Xiao, Z.; Chen, B.; Dai, J.; Hu, Y., Regeneration of Uterine Horns in Rats by Collagen Scaffolds Loaded with Collagen-binding Human Basic Fibroblast Growth Factor. *Biomaterials* **2011,** *32* (32), 8172-8181.
10. Xiao, B.; Yang, W.; Lei, D.; Huang, J.; Yin, Y.; Zhu, Y.; You, Z.; Wang, F.; Sun, S., PGS Scaffolds Promote the In Vivo Survival and Directional Differentiation of Bone Marrow Mesenchymal Stem Cells Restoring the Morphology and Function of Wounded Rat Uterus. *Advanced Healthcare Materials* **2019,** *8* (5), e1801455.
11. Magalhaes, R. S.; Williams, J. K.; Yoo, K. W.; Yoo, J. J.; Atala, A., A Tissue-engineered Uterus Supports Live Births in Rabbits. *Nature Biotechnology* **2020,** *38* (11), 1280-1287.
12. Wang, S.; Zhao, S.; Yu, J.; Gu, Z.; Zhang, Y., Advances in Translational 3D Printing for Cartilage, Bone, and Osteochondral Tissue Engineering. *Small* **2022,** *18* (36), e2201869.
13. Chen, S. S.; Shi, Y. F.; Zhang, X.; Ma, J., 3D Printed Hydroxyapatite Composite Scaffolds with Enhanced Mechanical Properties. *Ceramics International* **2019,** *45* (8), 10991-10996.
14. Mirkhalaf, M.; Men, Y.; Wang, R.; No, Y.; Zreiqat, H., Personalized 3D Printed Bone Scaffolds: A Review. *Acta Biomaterialia* **2023,** *156*, 110-124.

15. Yu, Q.; Wang, Q.; Zhang, L.; Deng, W.; Cao, X.; Wang, Z.; Sun, X.; Yu, J.; Xu, X., The Applications of 3D Printing in Wound Healing: The External Delivery of Stem Cells and Antibiosis. *Advanced Drug Delivery Reviews* **2023,** *197*, 114823.
16. Song, J.; Lv, B.; Chen, W.; Ding, P.; He, Y., Advances in 3D Printing Scaffolds for Peripheral Nerve and Spinal Cord Injury Repair. *International Journal of Extreme Manufacturing* **2023,** *5* (3).
17. Chen, S.; Shi, Y.; Zhang, X.; Ma, J., Biomimetic Synthesis of Mg-Substituted Hydroxyapatite Nanocomposites and Three-Dimensional Printing of Composite Scaffolds for Bone Regeneration. *Journal of Biomedical Materials Research Part A* **2019,** *107* (11), 2512-2521.
18. Ege, D.; Hasirci, V., Is 3D Printing Promising for Osteochondral Tissue Regeneration? *ACS Applied Bio Materials* **2023,** *6* (4), 1431-1444.
19. Nie, N.; Gong, L.; Jiang, D.; Liu, Y.; Zhang, J.; Xu, J.; Yao, X.; Wu, B.; Li, Y.; Zou, X., 3D Bio-Printed Endometrial Construct Restores the Full-Thickness Morphology and Fertility of Injured Uterine Endometrium. *Acta Biomaterialia* **2023,** *157*, 187-199.
20. Lu, S.; Wang, X.; Li, W.; Zu, Y.; Xiao, J., Injectable 3D-Printed Porous Scaffolds for Adipose Stem Cell Delivery and Endometrial Regeneration. *Advanced Functional Materials* **2023**.
21. Ji, W.; Hou, B.; Lin, W.; Wang, L.; Zheng, W.; Li, W.; Zheng, J.; Wen, X.; He, P., 3D Bioprinting A Human iPSC-Derived MSC-Loaded Scaffold for Repair of the Uterine Endometrium. *Acta Biomaterialia* **2020,** *116*, 268-284.
22. Jin, A.; Wang, Y.; Lin, K.; Jiang, L., Nanoparticles Modified by Polydopamine: Working as "Drug" Carriers. *Bioactive Materials* **2020,** *5* (3), 522-541.
23. Liu, Y.; Ai, K.; Liu, J.; Deng, M.; He, Y.; Lu, L., Dopamine-Melanin Colloidal Nanospheres: An Efficient Near-Infrared Photothermal Therapeutic Agent for In Vivo Cancer Therapy. *Advanced Materials* **2013,** *25* (9), 1353-1359.
24. Chen, S.; Wang, Y.; Zhang, X.; Ma, J.; Wang, M., Double-crosslinked Bifunctional Hydrogels with Encapsulated Anti-cancer Drug for Bone Tumor Cell Ablation and Bone Tissue Regeneration. *Colloids and Surfaces B: Biointerfaces* **2022,** *213*.
25. Chen, S.; Wang, Y.; Lai, J.; Tan, S.; Wang, M., Structure and Properties of Gelatin Methacryloyl (GelMA) Synthesized in Different Reaction Systems. *Biomacromolecules* **2023,** *24* (6), 2928-2941.
26. Hassan, M. N.; Yassin, M. A.; Eltawila, A. M.; Aladawi, A. E.; Mohamed-Ahmed, S.; Suliman, S.; Kandil, S.; Mustafa, K., Contact Osteogenesis by Biodegradable 3D-Printed Poly(lactide-co-trimethylene carbonate). *Biomaterials Research* **2022,** *26* (1), 55.
27. Chachlioutaki, K.; Karavasili, C.; Adamoudi, E.; Bouropoulos, N.; Tzetzis, D.; Bakopoulou, A.; Fatouros, D. G., Silk Sericin/PLGA Electrospun Scaffolds with Anti-Inflammatory Drug-eluting Properties for Periodontal Tissue Engineering. *Biomaterials Advances* **2022,** *133*, 112723.
28. Chen, Y.; Fei, W.; Zhao, Y.; Wang, F.; Zheng, X.; Luan, X.; Zheng, C., Sustained Delivery of 17beta-Estradiol by Human Amniotic Extracellular Matrix (HAECM) Scaffold Integrated with PLGA Microspheres for Endometrium Regeneration. *Drug Delivery* **2020,** *27* (1), 1165-1175.
29. Alves, N. M.; Pashkuleva, I.; Reis, R. L.; Mano, J. F., Controlling Cell Behavior Through

the Design of Polymer Surfaces. *Small* **2010,** *6* (20), 2208-2220.
30. Patntirapong, S.; Singhatanadgit, W.; Meesap, P.; Theerathanagorn, T.; Toso, M.; Janvikul, W., Stem Cell Adhesion and Proliferation on Hydrolyzed Poly(Butylene Succinate)/beta-Tricalcium Phosphate Composites. *Journal of Biomedical Materials Research Part A* **2015,** *103* (2), 658-670.
31. Owen, G. R.; Jackson, J.; Chehroudi, B.; Burt, H.; Brunette, D. M., A PLGA Membrane Controlling Cell Behaviour for Promoting Tissue Regeneration. *Biomaterials* **2005,** *26* (35), 7447-7456.
32. Xu, C.; Yang, F.; Wang, S.; Ramakrishna, S., In Vitro Study of Human Vascular Endothelial Cell Function on Materials with Various Surface Roughness. *Journal of Biomedical Materials Research Part A* **2004,** *71* (1), 154-161.
33. Schneider, M.; Fritzsche, N.; Puciul-Malinowska, A.; Balis, A.; Mostafa, A.; Bald, I.; Zapotoczny, S.; Taubert, A., Surface Etching of 3D Printed Poly(lactic acid) with NaOH: A Systematic Approach. *Polymers* **2020,** *12* (8).
34. Croll, T. I.; O'Connor, A. J.; Stevens, G. W.; Cooper-White, J. J., Controllable Surface Modification of Poly(lactic-co-glycolic acid) (PLGA) by Hydrolysis or Aminolysis I: Physical, Chemical, and Theoretical Aspects. *Biomacromolecules* **2004,** *5* (2), 463-473.
35. Joshi, S.; Mahadevan, G.; Verma, S.; Valiyaveettil, S., Bioinspired Adenine-Dopamine Immobilized Polymer Hydrogel Adhesives for Tissue Engineering. *Chemical Communications* **2020,** *56* (76), 11303-11306.
36. Li, H.; Jia, Y.; Peng, H.; Li, J., Recent Developments in Dopamine-based Materials for Cancer Diagnosis and Therapy. *Advances in Colloid and Interface Science* **2018,** *252*, 1-20.
37. Tomar, S.; Pandey, R.; Surya, P.; Verma, R.; Mathur, R.; Gangenahalli, G.; Singh, S., Multifunctional, Adhesive, and PDA-Coated Bioactive Glass Reinforced Composite Hydrogel for Regenerative Wound Healing. *ACS Biomaterials Science & Engineering* **2023,** *9* (3), 1520-1540.
38. Zhang, Y.; Lu, L.; Chen, Y.; Wang, J.; Chen, Y.; Mao, C.; Yang, M., Polydopamine Modification of Silk Fibroin Membranes Significantly Promotes Their Wound Healing Effect. *Biomater Sci* **2019,** *7* (12), 5232-5237.
39. Li, Y.; Liu, C.; Cheng, X.; Wang, J.; Pan, Y.; Liu, C.; Zhang, S.; Jian, X., PDA-BPs Integrated Mussel-Inspired Multifunctional Hydrogel Coating on PPENK Implants for Anti-Tumor Therapy, Antibacterial Infection and Bone Regeneration. *Bioactive Materials* **2023,** *27*, 546-559.
40. Wang, C.; Zhao, N.; Yuan, W., NIR/Thermoresponsive Injectable Self-Healing Hydrogels Containing Polydopamine Nanoparticles for Efficient Synergistic Cancer Thermochemotherapy. *ACS Applied Materials & Interfaces* **2020,** *12* (8), 9118-9131.
41. Hsieh, M. H.; Wang, T. H.; Hu, S. H.; Hsu, T. C.; Yow, J., L.,; Tzang, B., S.,; Chiang, W. H., Tumor Site-specific PEG Detachment and Active Tumor Homing of Therapeutic PEGylated Chitosan/Folate-decorated Polydopamine Nanoparticles to Augment Antitumor Efficacy of Photothermal/Chemo Combination Therapy. *Chemical Engineering Journal* **2022,** *446*.
42. Wang, Z.; Duan, Y.; Duan, Y., Application of Polydopamine in Tumor Targeted Drug Delivery System and Its Drug Release Behavior. *J Control Release* **2018,** *290*, 56-74.

43. Kou, L.; Jiang, X.; Xiao, S.; Zhao, Y. Z.; Yao, Q.; Chen, R., Therapeutic Options and Drug Delivery Strategies for the Prevention of Intrauterine Adhesions. *Journal of Controlled Release* **2020,** *318*, 25-37.
44. Liu, L.; Huang, X.; Xia, E.; Zhang, X.; Li, T. C.; Liu, Y., A Cohort Study Comparing 4 mg and 10 mg Daily Doses of Postoperative Oestradiol Therapy to Prevent Adhesion Reformation after Hysteroscopic Adhesiolysis. *Human Fertility* **2018,** *22* (3), 191-197.
45. Guo, J.; Li, T. C.; Liu, Y.; Xia, E.; Xiao, Y.; Zhou, F.; Yang, X., A Prospective, Randomized, Controlled Trial Comparing Two Doses of Oestrogen Therapy after Hysteroscopic Adhesiolysis to Prevent Intrauterine Adhesion Recurrence. *Reproductive Biomedicine Online* **2017,** *35* (5), 555-561.
46. Chen, S.; Shi, Y.; Luo, Y.; Ma, J., Layer-by-Layer Coated Porous 3D Printed Hydroxyapatite Composite Scaffolds for Controlled Drug Delivery. *Colloids and Surfaces B: Biointerfaces* **2019,** *179*, 121-127.
47. Wagberg, L.; Erlandsson, J., The Use of Layer-by-Layer Self-Assembly and Nanocellulose to Prepare Advanced Functional Materials. *Advanced Materials* **2021,** *33* (28), e2001474.
48. Chen, S.; Shi, Y.; Zhang, X.; Ma, J., Evaluation of BMP-2 and VEGF Loaded 3D Printed Hydroxyapatite Composite Scaffolds with Enhanced Osteogenic Capacity In Vitro and In Vivo. *Materials Science & Engineering C* **2020,** *112*, 110893.
49. Sarode, A.; Annapragada, A.; Guo, J.; Mitragotri, S., Layered Self-Assemblies for Controlled Drug Delivery: A Translational Overview. *Biomaterials* **2020,** *242*, 119929.
50. Howard, M. T.; Wang, S.; Berger, A. G.; Martin, J. R.; Jalili-Firoozinezhad, S.; Padera, R. F.; Hammond, P. T., Sustained Release of BMP-2 Using Self-Assembled Layer-By-Layer Film-Coated Implants Enhances Bone Regeneration over Burst Release. *Biomaterials* **2022,** *288*, 121721.
51. Yuan, W.; Weng, G. M.; Lipton, J.; Li, C. M.; Van Tassel, P. R.; Taylor, A. D., Weak Polyelectrolyte-based Multilayers via Layer-by-Layer Assembly: Approaches, Properties, and Applications. *Advances in Colloid and Interface Science* **2020,** *282*, 102200.
52. Guzman, E.; Rubio, R. G.; Ortega, F., A Closer Physico-Chemical Look to the Layer-by-Layer Electrostatic Self-assembly of Polyelectrolyte Multilayers. *Advances in Colloid and Interface Science* **2020,** *282*, 102197.
53. Hao, X.; Wang, W.; Yang, Z.; Yue, L.; Sun, H.; Wang, H.; Guo, Z.; Cheng, F.; Chen, S., pH Responsive Antifouling and Antibacterial Multilayer Films with Self-healing Performance. *Chemical Engineering Journal* **2019,** *356*, 130-141.
54. Baah-Dwomoh, A.; McGuire, J.; Tan, T.; De Vita, R., Mechanical Properties of Female Reproductive Organs and Supporting Connective Tissues: A Review of the Current State of Knowledge. *Applied Mechanics Reviews* **2016,** *68* (6).
55. Manoogian, S. J.; Bisplinghoff, J. A.; Kemper, A. R.; Duma, S. M., Dynamic Material Properties of the Pregnant Human Uterus. *Journal of Biomechanics* **2012,** *45* (9), 1724-1727.
56. Wang, W.; Tang, Z.; Zhang, Y.; Wang, Q.; Liang, Z.; Zeng, X., Mussel-Inspired Polydopamine: The Bridge for Targeting Drug Delivery System and Synergistic Cancer Treatment. *Macromolecular Bioscience* **2020,** *20* (10), e2000222.
57. An, Q.; Huang, T.; Shi, F., Covalent Layer-by-Layer Films: Chemistry, Design, and Multidisciplinary Applications. *Chemical Society Reviews* **2018,** *47* (13), 5061-5098.

58. Janzen, D. M.; Cheng, D.; Schafenacker, A. M.; Paik, D. Y.; Goldstein, A. S.; Witte, O. N.; Jaroszewicz, A.; Pellegrini, M.; Memarzadeh, S., Estrogen and Progesterone Together Expand Murine Endometrial Epithelial Progenitor Cells. *Stem Cells* **2013,** *31* (4), 808-822.
59. Johary, J.; Xue, M.; Zhu, X.; Xu, D.; Velu, P. P., Efficacy of Estrogen Therapy in Patients with Intrauterine Adhesions: Systematic Review. *Journal of Minimally Invasive Gynecology* **2014,** *21* (1), 44-54.
60. Yao, Q.; Zheng, Y. W.; Lan, Q. H.; Wang, L. F.; Huang, Z. W.; Chen, R.; Yang, Y.; Xu, H. L.; Kou, L.; Zhao, Y. Z., Aloe/Poloxamer Hydrogel as An Injectable Beta-estradiol Delivery Scaffold with Multi-therapeutic Effects to Promote Endometrial Regeneration for Intrauterine Adhesion Treatment. *European Journal of Pharmaceutical Sciences* **2020,** *148*, 105316.
61. Zhang, S. S.; Xu, X. X.; Xiang, W. W.; Zhang, H. H.; Lin, H. L.; Shen, L. E.; Lin, Q.; Lin, F.; Zhou, Z. Y., Using 17Beta-estradiol Heparin-Poloxamer Thermosensitive Hydrogel to Enhance the Endometrial Regeneration and Functional Recovery of Intrauterine Adhesions in A Rat Model. *The FASEB Journal* **2020,** *34* (1), 446-457.
62. Xin, L.; Zheng, X.; Chen, J.; Hu, S.; Luo, Y.; Ge, Q.; Jin, X.; Ma, L.; Zhang, S., An Acellular Scaffold Facilitates Endometrial Regeneration and Fertility Restoration via Recruiting Endogenous Mesenchymal Stem Cells. *Advanced Healthcare Materials* **2022,** *11* (21), e2201680.
63. Ouyang, L. L.; Armstrong, J. P. K.; Lin, Y. Y.; Wojciechowski, J. P.; Lee-Reeves, C.; Hachim, D.; Zhou, K.; Burdick, J. A.; Stevens, M. M., Expanding and Optimizing 3D Bioprinting Capabilities Using Complementary Network Bioinks. *Science Advances* **2020,** *6* (38), eabc5529.
64. Yi, S.; Liu, Q.; Luo, Z.; He, J. J.; Ma, H. L.; Li, W.; Wang, D.; Zhou, C.; Garciamendez, C. E.; Hou, L.; Zhang, J.; Zhang, Y. S., Micropore-Forming Gelatin Methacryloyl (GelMA) Bioink Toolbox 2.0: Designable Tunability and Adaptability for 3D Bioprinting Applications. *Small* **2022,** *18* (25), e2106357.
65. Torii, H.; Takagi, T.; Urabe, M.; Tsujimoto, H.; Ozamoto, Y.; Miyamoto, H.; Ikada, Y.; Hagiwara, A., Anti-adhesive Effects of A Newly Developed Two-layered Gelatin Sheet in Dogs. *Journal of Obstetrics and Gynaecology Research* **2017,** *43* (8), 1317-1325.
66. Zambuto, S. G.; Clancy, K. B. H.; Harley, B. A. C., A Gelatin Hydrogel to Study Endometrial Angiogenesis and Trophoblast Invasion. *Interface Focus* **2019,** *9* (5), 20190016.
67. Gladman, A. S.; Matsumoto, E. A.; Nuzzo, R. G.; Mahadevan, L.; Lewis, J. A., Biomimetic 4D Printing. *Nature Materials* **2016,** *15* (4), 413-418.
68. Champeau, M.; Heinze, D. A.; Viana, T. N.; de Souza, E. R.; Chinellato, A. C.; Titotto, S., 4D Printing of Hydrogels: A Review. *Adv. Funct. Mater.* **2020,** *30* (31).
69. Wu, Z.; Su, X.; Xu, Y.; Kong, B.; Sun, W.; Mi, S., Bioprinting Three-Dimensional Cell-Laden Tissue Constructs with Controllable Degradation. *Scientific Reports* **2016,** *6*, 24474.

Supporting Information

Multilayered Shape-morphing Scaffolds with a Hierarchical Structure for Uterine Tissue Regeneration

Shangsi Chen [a, 1], Shenglong Tan [b, 1], Liwu Zheng [c], Min Wang [a, *]

[a] Department of Mechanical Engineering
The University of Hong Kong
Pokfulam Road, Hong Kong

[b] Department of Endodontics and Operative Dentistry
College of Stomatology, Southern Medical University
No. 1838 North Guangzhou Avenue, Guangzhou, China

[c] Faculty of Dentistry
The University of Hong Kong
34 Hospital Road, Sai Ying Pun, Hong Kong

[1] These authors contributed equally to this work.

* Correspondence to:
Professor Min Wang at the University of Hong Kong, Hong Kong
Email: memwang@hku.hk Tel: +852 3917 7903 Fax: +852 2858 5415

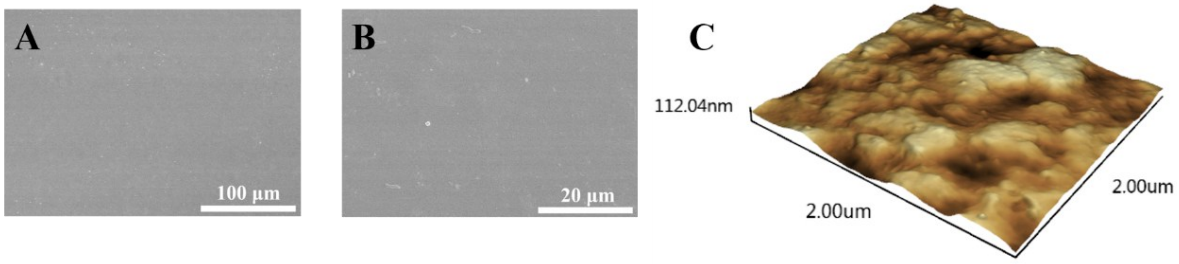

Fig.S1 Surface morphology of M scaffolds. (A) and (B) SEM images of M scaffolds. (C) Atomic force microscope (AFM) image of an M scaffold.

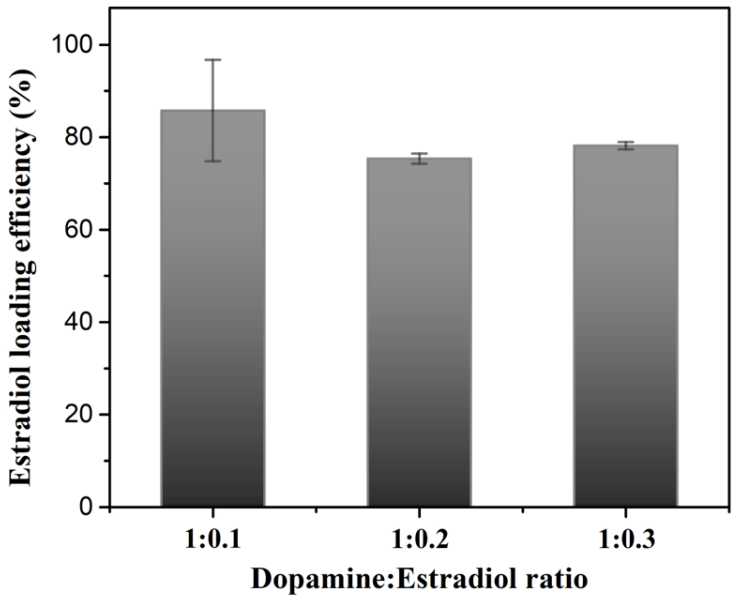

Fig.S2 E2 loading efficiency of PDA particles with different dopamine to E2 ratios.

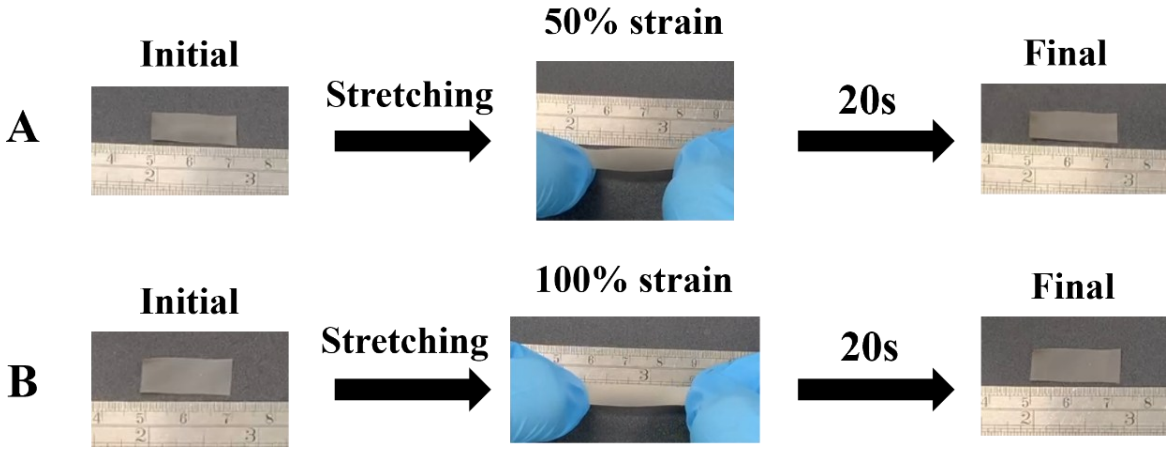

Fig.S3 Recovery of M-N-(PDA@E2/HA)$_{20}$ scaffolds after stretching to (A) 50% strain and (B) 100% strain, respectively.

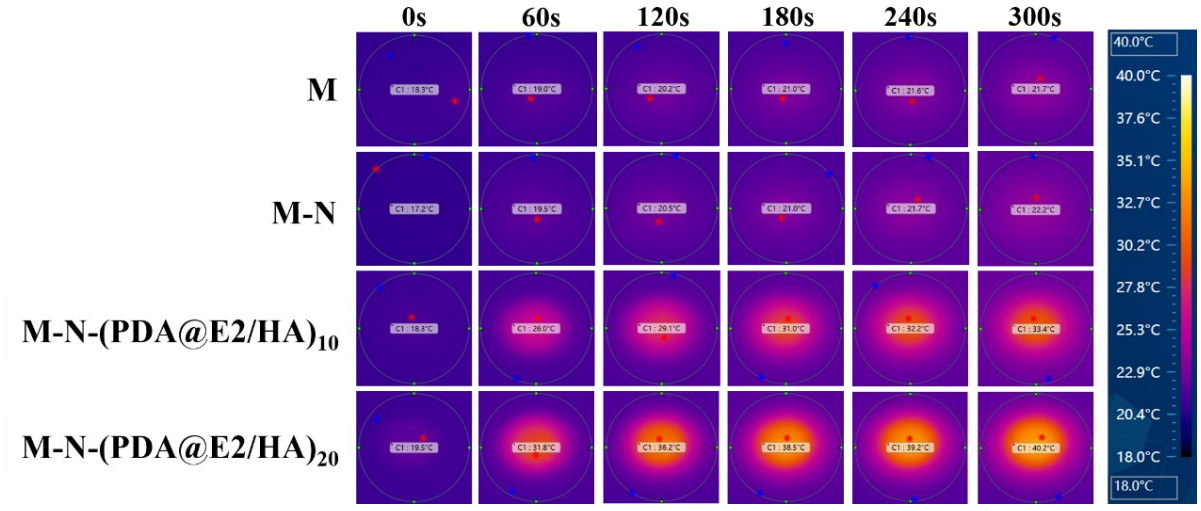

Fig.S4 Infrared thermal images of M, M-N, M-N-(PDA@E2/HA)$_{10}$, and M-N-(PDA@E2/HA)$_{20}$ scaffolds under the irradiation of an 808nm wavelength NIR laser at the power density of 1.0 W/cm^2 for different times.

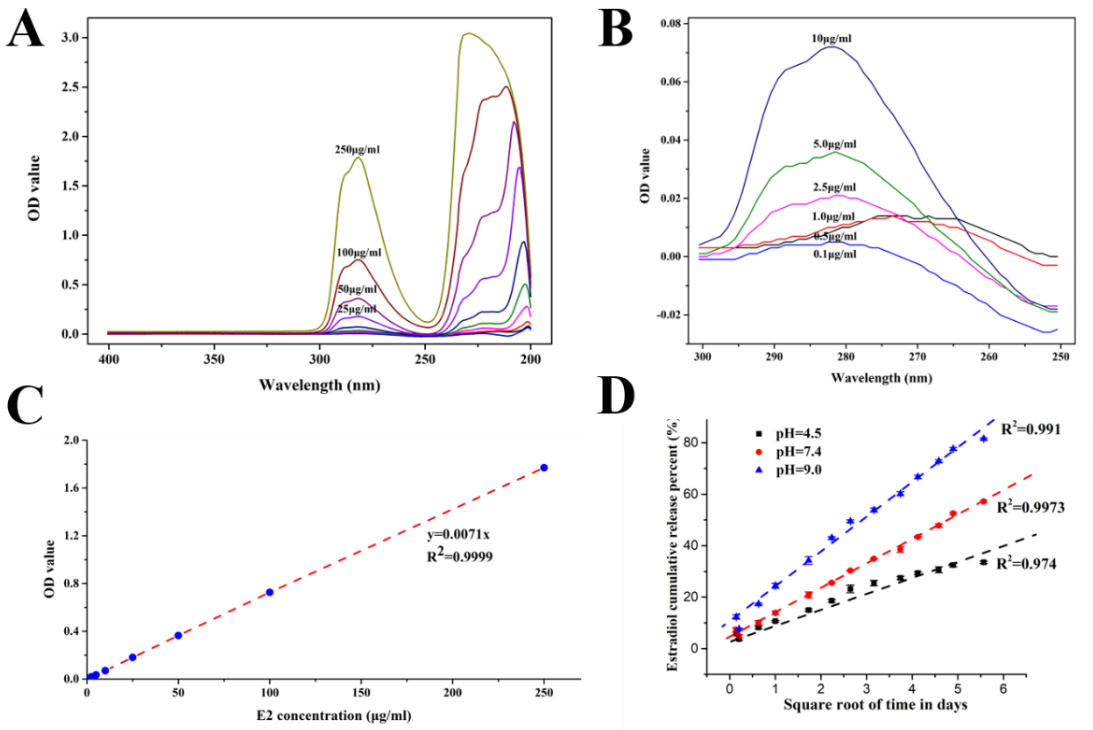

Fig.S5 (A) and (B) Optical density (OD) values of solutions of different E2 concentrations as measured by a UV-vis spectrometer. (C) Calibration curve for OD values (at 280nm wavelength) and E2 concentrations. (D) Application of the Higuchi model for E2 release from M-N-(PDA@E2/HA)$_{20}$ scaffolds.

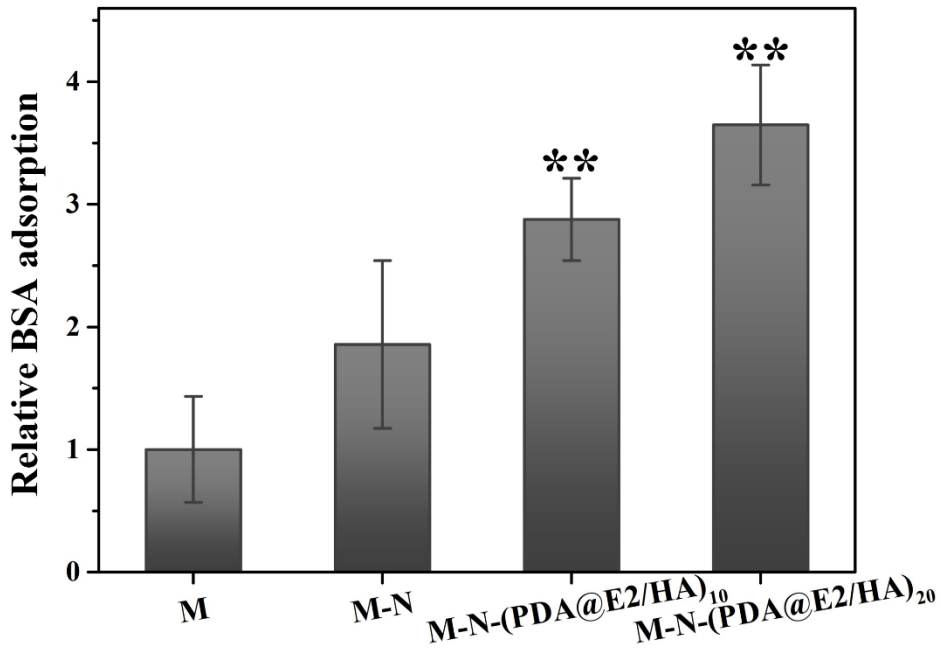

Fig.S6 BSA adsorption by M, M-N, M-N-(PDA@E2/HA)$_{10}$, and M-N-(PDA@E2/HA)$_{20}$ scaffolds.

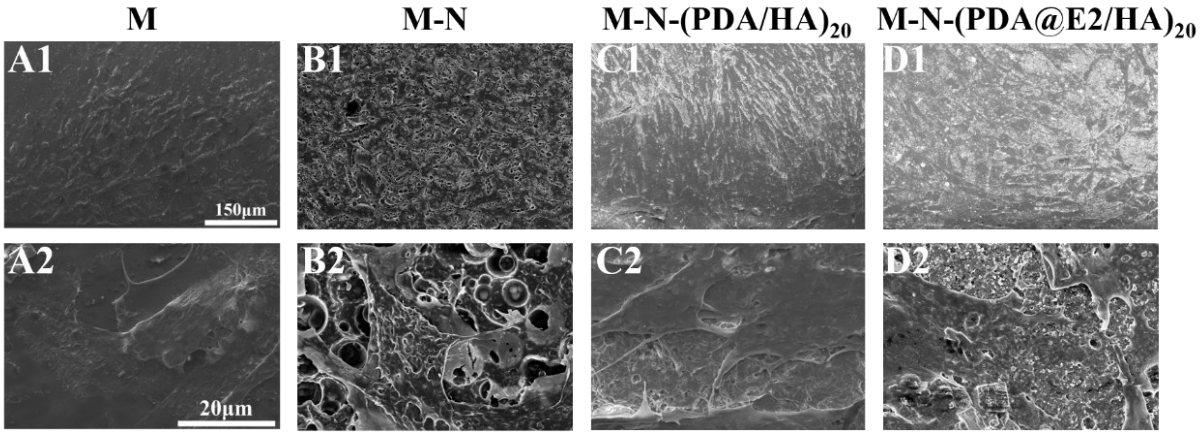

Fig.S7 SEM images showing the morphology of BMSCs cultured on (A1, A2) M, (B1, B2) M-N, (C1, C2) M-N-(PDA/HA)$_{20}$, and (D1, D2) M-N-(PDA@E2/HA)$_{20}$ scaffolds.

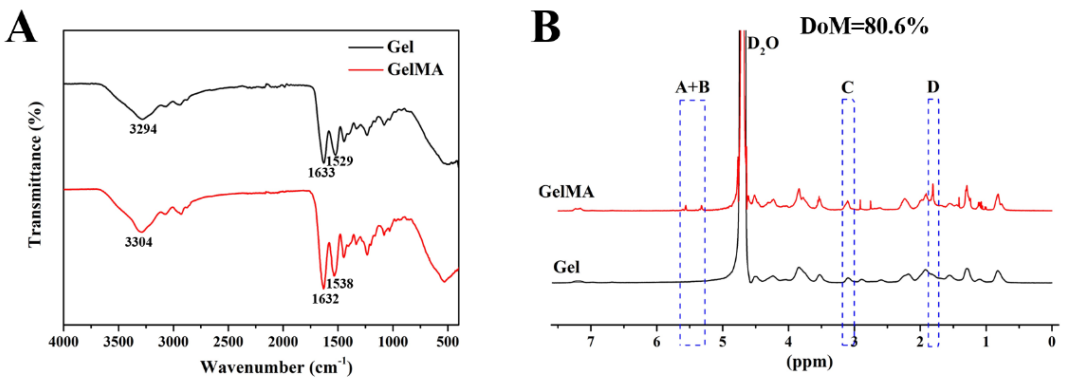

Fig.S8 Characteristics of synthesized GelMA and Gel. (A) FT-IR spectra, (B) ^{1}H-NMR spectra.

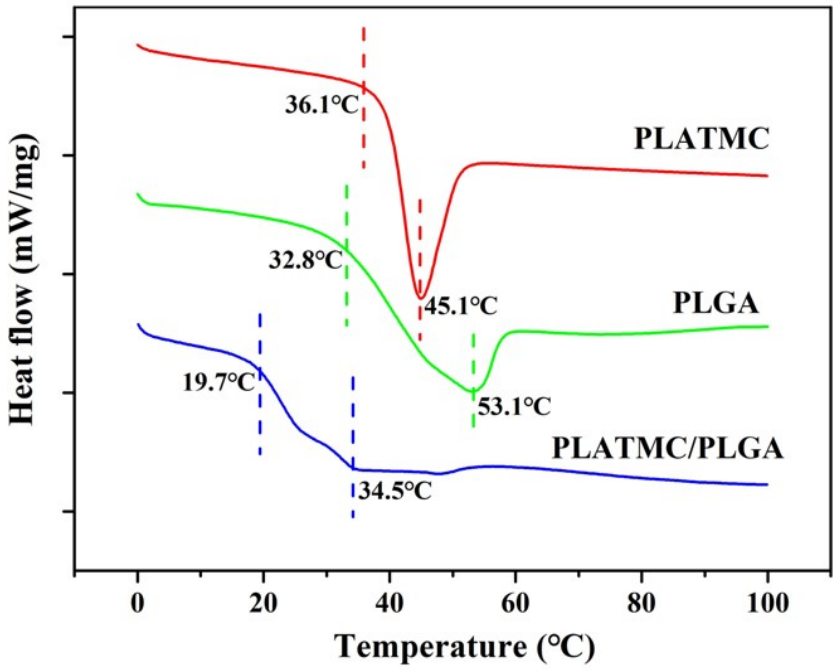

Fig.S9 DSC curves for PLATMC, PLGA and PLATMC/PLGA.

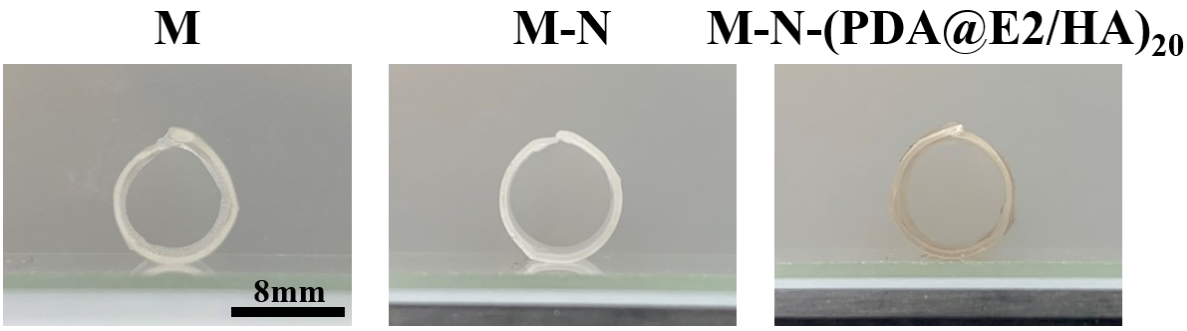

Fig.S10 Tubular structures of M, M-N, and M-N-(PDA@E2/HA)$_{20}$ scaffolds evolved from the original planar shape after being immersed in a 37℃ water bath.

Table S1 Tensile properties of M, M-N, M-N-(PDA@E2/HA)$_{10}$, and M-N-(PDA@E2/HA)$_{20}$ scaffolds.

Scaffold	Elastic Strain (%)	Yield Strength (MPa)	Elastic Modulus (MPa)	Ultimate Strength (MPa)	Elongation at Break (%)	Fracture Strength (MPa)
M	1.03±0.12	0.25±0.063	6.92±0.82	0.83±0.12	514.01±11.13	0.74±0.17
M-N	4.94±0.44	0.29±0.0071	4.38±0.49	0.89±0.057	501.42±29.99	0.38±0.18
M-N-(PDA/HA)$_{10}$	4.32±0.54	0.49±0.12	13.46±2.28	13.46±2.28	13.46±2.28	0.98±0.28
M-N-(PDA/HA)$_{20}$	4.45±0.09	0.50±0.06	15.09±7.33	1.62±0.12	501.37±22.98	1.24±0.25